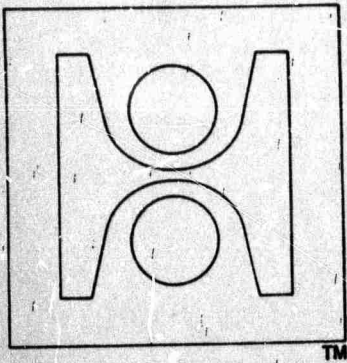


AD 733050



TM

S.O. No. 3212

SECOND HARMONIC GENERATION

FINAL TECHNICAL REPORT

OCTOBER 1971

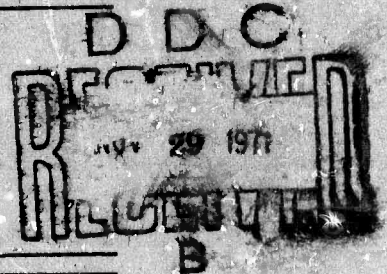
Prepared by

James H. Boyden
Edward G. Erickson
James E. Murray
Robert Webb

Office of Naval Research

Contract No. N00014-71-C-0044
Program Code No. 421

1 September 1970 through 3 August 1971



Sponsored by
Advanced Research Projects Agency
ARPA Order No. 306

Reproduced by
**NATIONAL TECHNICAL
INFORMATION SERVICE**
Springfield, Va. 22151



HOLOBEAM[®], INC.

560 WINTERS AVENUE ■ PARAMUS, NEW JERSEY 07652
TEL. 201-265-5335 ■ TWX. 710-990-4957

85



HOLOBEAM, INC.

SECOND HARMONIC GENERATION
Final Technical Report
October 1971

ONR Contract No. N00014-71-C-0044
Program Code No. 421

Sponsored by
Advanced Research Projects Agency
ARPA Order No. 306

The Scientific Officer under this contract is the Director,
Physics Programs, Physical Sciences Division, Office of
Naval Research, Department of the Navy, Washington, D. C.
20360.

Duration of Contract 9/1/70 to 8/3/71
Amount of Contract \$97,066.00

Prepared by

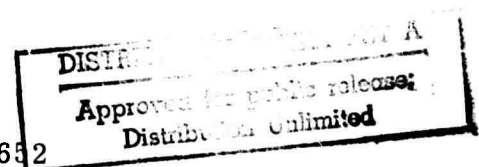
James H. Boyden
Edward G. Erickson

James E. Murray
Robert Webb

This research was supported by the Advanced
Research Projects Agency of the Department
of Defense and was monitored by ONR under
Contract No. N00014-71-C-0044.

The views and conclusions contained in this document
are those of the authors and should not be interpreted
as necessarily representing the official policies,
either expressed or implied, of the Advanced Research
Projects Agency or the U. S. Government.

HOLOBEAM, INC.
560 WINTERS AVENUE
PARAMUS, NEW JERSEY 07652
Telephone 265-5335



DOCUMENT CONTROL DATA - R & D

(Security classification of title, body of abstract and indexing annotation must be entered when the overall report is classified)

1. ORIGINATING ACTIVITY (Corporate author) Holobeam, Inc.		2a. REPORT SECURITY CLASSIFICATION Unclassified	
		2b. GROUP	
3. REPORT TITLE SECOND HARMONIC GENERATION			
4. DESCRIPTIVE NOTES (Type of report and inclusive dates) Final Technical Report 1 Sept 1970 through 3 Aug 1971			
5. AUTHOR(S) (Last name, first name, initial) Boyden, James H. Murray, James E. Erickson, Edward G. Webb, Robert			
6. REPORT DATE October 1971		7a. TOTAL NO. OF PAGES 84	7b. NO. OF REFS 4
8a. CONTRACT OR GRANT NO. N00014-71-C-0044		8b. ORIGINATOR'S REPORT NUMBER(S) Holobeam No. 3212	
b. PROJECT NO.		9b. OTHER REPORT NO(S) (A1/ other numbers that may be assigned this report)	
c. Program Code No. 421			
d.			
10. DISTRIBUTION STATEMENT			
11. SUPPLEMENTARY NOTES		12. SPONSORING MILITARY ACTIVITY Advanced Research Projects Agency ARPA Order No. 306	
13. ABSTRACT The investigations under the subject contract had the objectives of producing high average powers in a Second Harmonic Generation laser system at a wavelength of 0.532 microns with a short pulse and high repetition frequency format. The program's objectives were to be achieved by using a high average power CW Nd:YAG laser combined with electric-optical Q-switching techniques and mode-locked pulse injection as a source of 1.065 micron power drive to a nonlinear crystal. Both well known and new materials were investigated in order to achieve high conversion efficiencies. Damage and the thermal failure of materials was an area of special concern in this program.			

14. KEY WORDS	LINK A		LINK B		LINK C	
	ROLE	WT	ROLE	WT	ROLE	WT
Lasers Second Harmonic Generation Mode-Lock Nd:YAG Laser Q-Switch Pockels Cell Frequency Doubling						



TABLE OF CONTENTS

<u>Section</u>	<u>Title</u>	<u>Page</u>
I	INTRODUCTION.	1
II	LASER SYSTEM.	3
	2.1 Q-Switched Operation.	3
	2.2 Mode-Locked Injection Technique	10
	2.3 Switching Electronics.	15
III	NON-LINEAR MATERIALS.	18
	3.1 Nonlinear Crystal Survey	18
	3.2 Optical Absorption Measurement.	20
	3.3 Phase-Match Temperature and Efficiency of the Arsenates	28
	3.4 CsD ₂ AsO ₄ Temperature Phase-Matching	30
IV	SECOND HARMONIC GENERATION AT HIGH AVERAGE POWER.	35
	4.1 SHG Apparatus and Tests	35
V	SOME THEORETICAL CONSIDERATIONS	50
	5.1 Crystal Heating Due to Super Non Linear Effects.	50
	5.2 Phase-Match Degradation Due to Absorption.	67
	5.3 Pulse Width Degradation.	69
VI	CONCLUSIONS	72
VII	SUGGESTIONS FOR CsD ₂ AsO ₄ CRYSTAL IMPROVEMENT.	75
	REFERENCES	78



LIST OF ILLUSTRATIONS

<u>Figure No.</u>	<u>Title</u>	<u>Page</u>
2-1	Output vs Input Curves for Multiple Nd:YAG Laser Heads.	4
2-2	Schematic Drawing of Polarizing Technique for CW Operation of Series 2500-8 Nd:YAG Laser	6
2-3	Schematic Drawing of "Q" Switching Technique	8
2-4	Single Trace of Q-Switched Output from Series 2500 8-Stage Laser System	11
2-5	Detail Schematic of Series 250 Mode-Locked Laser	12
2-6	Multiple Traces showing Difference Between Normal "Q" Switched Output and "Q" Switched with Open Loop Mode-Locking Output at Equal Energy per Pulse.	14
2-7	Detail Schematic of Complete Q-Switched and Mode-Locked and Frequency-Doubled Series 2500 8-Stage Laser System	16
2-8	Oscilloscope Traces of Closed Loop Mode-Locked "Q" Switched	17
3-1	Construction of Peltier Device	22
3-2	Closeup of Thermo-Electric Cooler Assembly	23
3-3	Peltier Cooler Calibration Curve	25
3-4	Transmission Curves for Deuterated Crystals	29
3-5	CDA Efficiency Versus Power Density for Pulsed Operation	31
3-6	Oven Assembly for Testing Phase-Match Temperature of 90° Phase-Matchable SHG Materials.	32
3-7	CsD ₂ AsO ₄ Phase-Match Versus Temperature	34
4-1	Experimental Arrangement of Complete System.	36
4-2	Experimental Arrangement of Complete System.	37
4-3	Mode-Locking Electronics for 77MHz	38
4-4	Variable "Trombone" for Phase Control of 77MHz A. F. Signal	39
4-5	Series 250 Mode-Locked/Series 2500-8 Laser System.	40
4-6	"Q" Switch Pockels Cell Assembly in Position Between Last Stage of Series 2500-8 Laser and Mirror Common with the Series 250 Mode-Locked Laser	41



LIST OF ILLUSTRATIONS (Cont'd)

<u>Figure No.</u>	<u>Title</u>	<u>Page</u>
4-7	Output of Laser System is through Lens at Upper Left then through Frequency Doubling Oven/Cell Windows and SHG Material.	42
4-8	Pulses per Second at Constant Input Energy/Pulse of 100mJ.	46
4-9	Measured Single Pass Efficiency of SHG Materials	47

LIST OF TABLES

<u>Table No.</u>	<u>Title</u>	<u>Page</u>
I	Nonlinear Crystal Selection	19
II	Percentage Absorption per Centimeter of Length for Nonlinear Crystal Specimens.	26
III	Averaged Percentage Absorption for Nonlinear Crystals Tested.	27



SECTION I

INTRODUCTION

This technical report summarizes the research and development efforts on Contract No. N00014-71-C-0044. This program was directed toward the attainment of high average powers at a wavelength of 0.532 microns, with a short pulse, high repetition frequency format. The program's objectives were to be achieved by utilizing a high average power CW Nd:YAG laser combined with electro-optic Q-switching techniques and mode-locked pulse injection as a source of 1.065 micron power to drive a nonlinear crystal. Both well known and new materials were to be investigated in order to achieve high conversion efficiencies. Damage and the thermal failure of materials was an area of special concern in this program.

Our approach to the generation of high average second harmonic powers has been to develop a high average power 1.065 microns source which emits its output in a high repetition frequency high peak power format. We have accomplished this by utilizing the HoloBeam developed 1000 watt CW Nd:YAG laser in conjunction with a unique electro-optical Q-switching technique combined with the injection of ultra-short pulses from a CW mode-locked Nd:YAG laser.

In order to optimally utilize the multitransverse mode output from this laser we have emphasized the utilization of 90° phase-matching nonlinear materials for conversion of the 1.065 micron radiation into its second harmonic. Since the well known materials barium sodium niobate and lithium niobate have exhibited rather low damage thresholds, and potassium dideuterious phosphate does not 90° phase match, we have explored in some detail the use of a new material, cesium dideuterium arsenate.

It has been demonstrated that cesium dideuterium arsenate is an efficient second harmonic converter when used in the 90° phase-matching direction and operated at the phase-match temperature of approximately 100°C . In excess of 25% conversion has been demonstrated for multimode polarized up conversion from 1.06μ to 0.53μ in a one cm length (single pass). It has further been shown that efficiencies in excess of 40% for a single pass can be obtained in a one cm length of this material when greater mode-locking enhancement is utilized. No surface damage has been observed at non-mode-locked power densities of up to 300 mW/cm^2 . 1.8 watts average green output power has been observed at a repetition rate of 100 pps and



7.2 watts average green output power has been observed at 800 pps utilizing this technique. The effect on conversion efficiency of crystal heating due to fundamental absorption has been clearly demonstrated.

A basic problem inherent in "high efficiency" frequency doubling materials has been discovered which seriously limits the use of some of these materials, such as barium sodium niobate, to the relatively unimportant role of providing efficiencies of only a few percent single pass at low power densities. This basic problem is a saturation effect which can cause the frequency doubled output to limit or actually decrease as a function of increasing power density at phase-match temperatures and at conversion efficiencies of about 12% single pass for a 5 mm length and power density of 10 mW/cm^2 . It is believed that this saturation effect is in reality a two-photon absorption process wherein one photon at 1.06μ and one photon at 0.53μ is absorbed into the absorption band edge at 0.35μ . Evidence is presented later in this section supporting this conclusion. It is further speculated that this two-photon absorption process may be the basic cause of the surface damage seen with barium sodium niobate at the relatively low power densities of one or two MW/cm^2 at phase-match temperature. (Air Force Contract No. : F 33615-69-C-1841)

Barium sodium niobate, lithium niobate, potassium dideuterium phosphate and cesium dideuterium arsenate (CD*A) have all been tested as high average power harmonic generators. No material has shown a single pass SHG efficiency higher than 14% at any power density, with the exception of CD*A, when utilizing a high divergence (10 mR) multimode pump source in spite of the theoretical difference in basic SHG efficiency of a factor of 2000 between barium sodium niobate and CD*A (per unit length and unit power density).

The laser source has been developed to the point where peak powers on the order of 5 MW are typical at pulse repetition rates in excess of 800 pps and average power outputs in excess of 80 watts. This represents pulse energies of 100 mJ/pulse. The mode-locking pulse injection system is able to provide SHG enhancement of up to a factor of 5.



SECTION II

LASER SYSTEM

The laser system utilized in this development program is an eight stage, single ellipse, krypton arc lamp pumped Nd:YAG laser which has produced an output in excess of 1100 watts C. W. at 1.06 microns with an input power of 48 kilowatts. The laser developed under a HoloBeam internally supported program, contains 8 Nd:YAG rods, each of which are $\frac{1}{4}$ " in diameter and 3 inches long. Each stage contains one rod, a single ellipse and a single pump lamp which is capable of an input power of 6kW. In the interest of a reasonable lamp lifetime, a maximum input of 5kW is normally utilized which provides an output for all eight stages of between 760 and 800 watts. Output curves are shown in Figure 2-1.

The typical beam divergence at 800 watts is 15mR, although a beam divergence of 5mR was obtained at an output power of 500 watts, utilizing a slightly modified version. The overall dimensions of the laser head chain are 4 inches x 4 inches x 62 inches.

2.1 Q-Switched Operation

The problems associated with "Q" switching a continuously pumped Nd:YAG laser are primarily caused by an induced thermo-optic birefringence which becomes more severe as the pumping power and presumably the C. W. output power is increased in any given system. This birefringence in most cases eliminates or at least severely limits the utilization of a Pockels cell as the "Q" switching mechanism due to the basic requirement that the laser must be internally polarized. We report here on a technique which utilizes this birefringence as an output coupling mechanism for a C. W. pumped laser which has both a high gain and a high coupling coefficient between states of polarization, that is, a high degree of birefringence.

We have measured the single pass gain of the system at a pump level of 5kW/lamp by inserting a one-half watt C. W. beam from another YAG laser after removing the mirrors from the main system. The measured output was 8 watts, implying a single pass small signal gain of 16 and a double pass gain of 256 which is

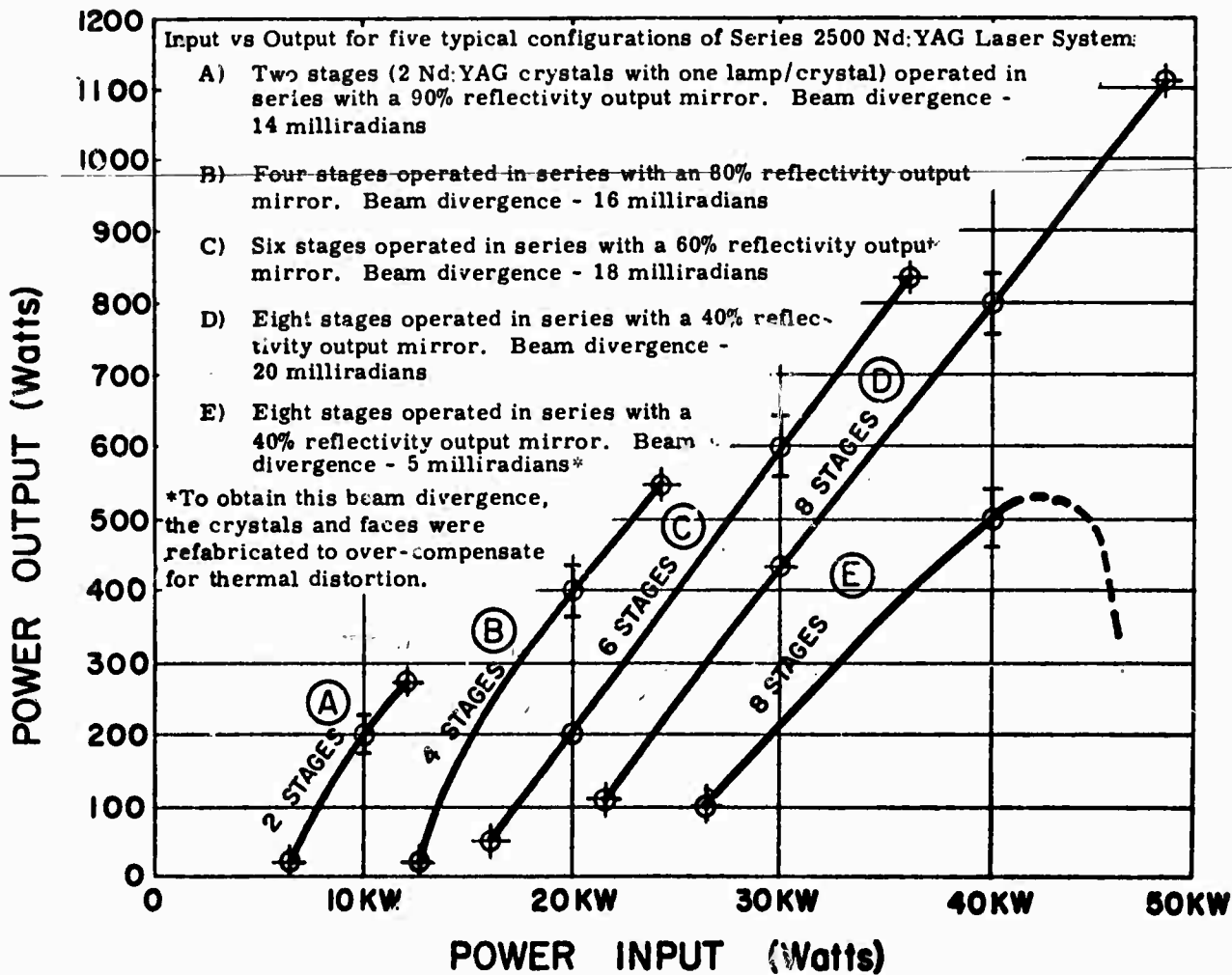


FIGURE 2-1

Output vs Input Curves for Multiple Nd:YAG Laser Heads



consistent with the empirically determined optimum output coupling of 65%. In other words a 35% reflecting output mirror has been found to provide the highest output in the C. W. case. As an additional check on round trip gain, a single surface of a quartz wedge that had been A. R. coated and checked for a reflectivity of less than .2% was used in place of the normal 35% R output mirror and threshold lasing was achieved at 6kW/lamp implying a total round trip gain of greater than 500.

With round trip gains of this magnitude most normal techniques for "Q" switching a C. W. YAG laser such as an acousto-optical cell are inappropriate since the highest depth of modulation achieved in such a device utilizing quartz as the active medium is only on the order of 50%. A mechanical Q-switch is also inappropriate due to the high rotational speeds that would be required. We therefore decided that a Pockels cell was the only way we could achieve the switching times, repetition rates and depths of modulation necessary, and we have in fact devised a means to accomplish this.

Figure 2-2 depicts schematically the method utilized to separate one of the states of polarization. Item A is the end of the last rod in the laser system. Item B is a 90° polarizing prism oriented in such a way that the hypotenuse of the right triangle shown is at 18° to the optic axis through the laser. Item C is a 100% reflecting mirror at 1.06 microns and is placed normal to the reflected beam.

Surface "A" of the prism has been multi-layer coated for an "S" wave reflectivity of 73% at 18° to the optical axis and a "P" wave transmission in excess of 99%. This means that portion of the beam which is reflected is essentially totally polarized. The output beam exits through the prism and is within a few degrees of normal to the exit surface so that an A. R. coating is used effectively on that surface as well as on the third surface. Let us consider an unpolarized beam leaving the laser rod. As the beam strikes the polarizing surface, that portion which corresponds in polarity to the "P" wave passes through the prism without loss. This power represents 50% of the total available. That portion of the beam which corresponds to the "S" wave is split so that 27% of the S wave passes through the prism also. Therefore a total of 63-1/2% which is totally

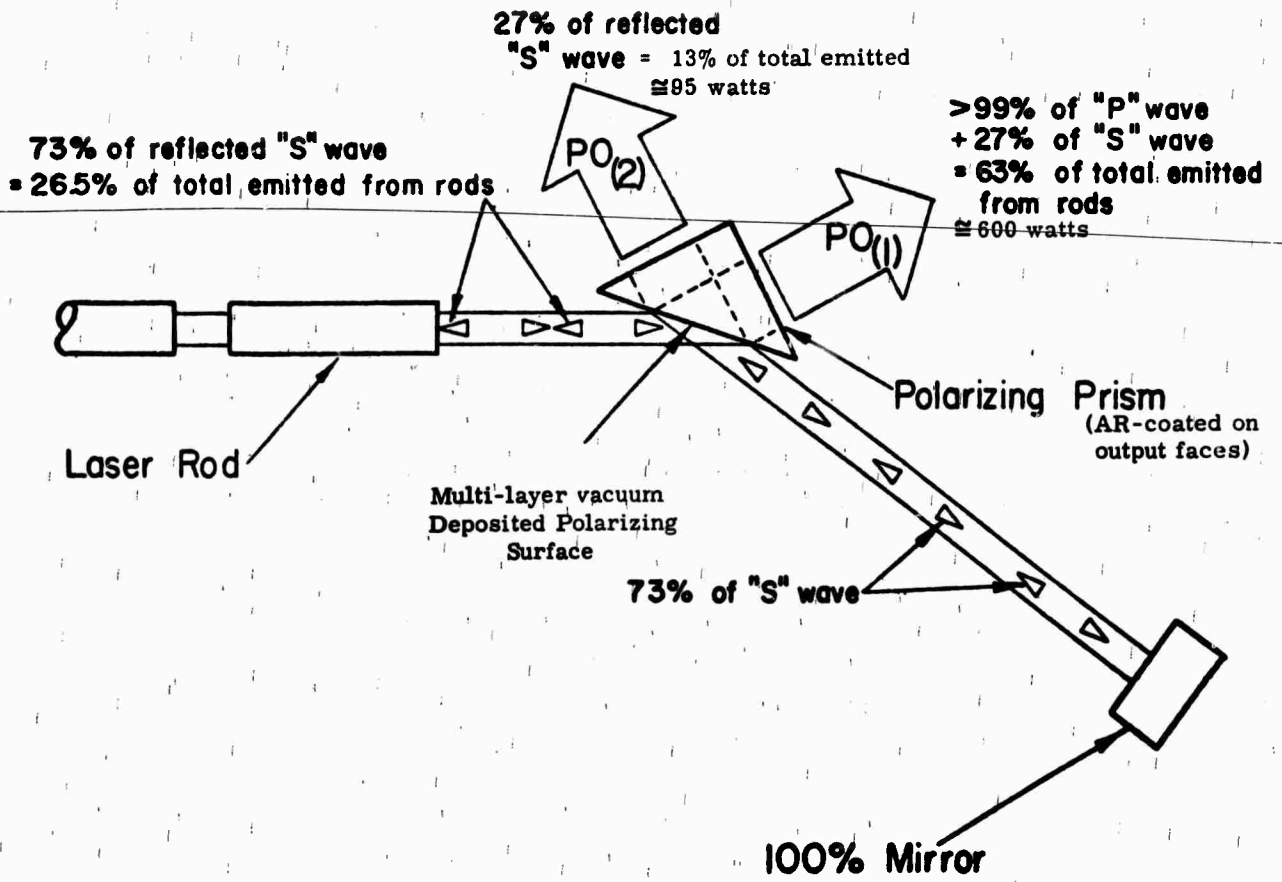


FIGURE 2-2

Schematic Drawing of Polarizing Technique for CW Operation of Series 2500-8 Nd:YAG Laser



polarized in the S direction, is reflected from the 100% mirror and directed back to the polarizer, at which point 27% passes through the polarizer and 73% is reflected back into the laser. This 73% represents only about 26-1/2% of the total power emitted originally. Therefore the laser effectively has an output mirror reflectivity of only 26-1/2%. Now, to recap the distribution of power in this device, assume a total unpolarized power emitted from the end of the rod of 1,000 watts, 635 watts will be emitted in the primary beam (P_{o1}), 99 watts will be emitted in the secondary beam (P_{o2}) and 266 watts will be returned to the laser. All of this 266 watts is polarized in the S wave direction as it initially enters the laser rods. However as the beam passes through the rods and is amplified it encounters strong birefringence and by the time it has made the complete round trip through the laser, the beam polarity is again totally scrambled or unpolarized and at a power level equal to the original 1,000 watts. In operation we have observed slightly over 600 watts C. W. out in the primary beam (P_{o1}) and 95 watts out in the secondary beam (P_{o2}) at normal input power.

If we block the S wave leg of the split beam the laser stops emitting since there is no reflecting surface normal to the beam. Therefore if we place a second polarizer oriented in such a way as to create a crossed condition in the S wave leg, we also completely stop the system from lasing. We now have an ideal situation for inserting a Pockels cell between the crossed polarizers. If we operate the cell in the pulse voltage on condition, i. e. if we apply a half-wave voltage to the cell, the system will oscillate.

Figure 2-3 shows the apparatus used to accomplish "Q" switching using this technique. The letter A denotes the prism, the letter B denotes the Pockels cell, C is the second polarizer (a coated plate), D is the 100% reflecting mirror, $P_{o(1)}$ is the primary output beam and $P_{o(2)}$ is the secondary output beam.

A single surface polarizer, obtained from the Valpey Corporation, utilized a multilayer dielectric coating to provide a separation of the two states of polarization intracavity. The polarizer is a 90° quartz prism with the polarizing surface applied on the hypotenuse.

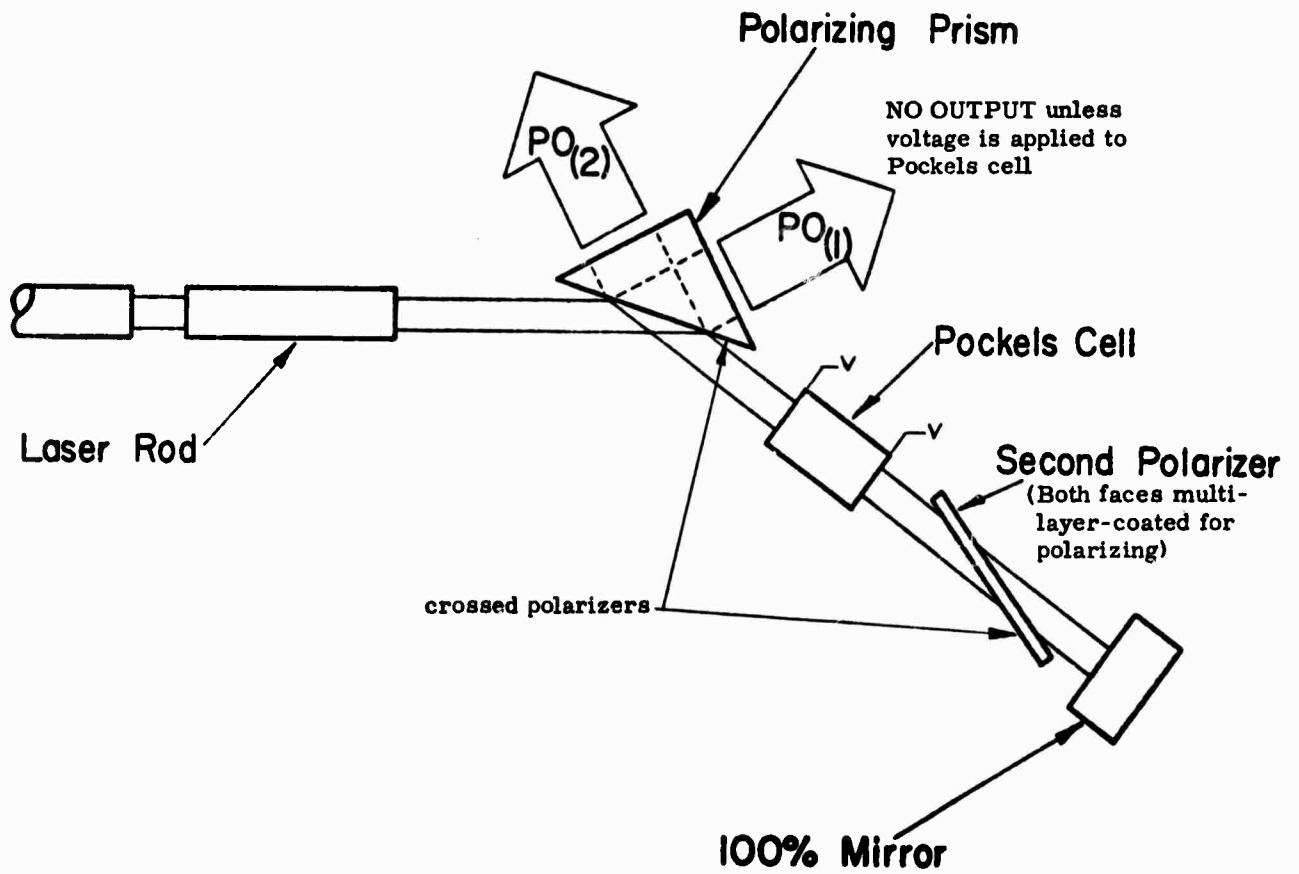


FIGURE 2-3

Schematic Drawing of "Q" Switching Technique



The other two surfaces are A. R. coated for 1.06 microns since a beam is emitted from both surfaces. The prism must be set in the system at an angle of incidence of 72° with respect to the optical axis of the laser. A single maximum reflectivity mirror was aligned with the reflected beam.

The second polarizer was a wedged fused quartz plate dielectric coated on both sides with the same characteristics as the prism polarizer. After two passes through the polarizer the residual value of the undesired component is only 5.3×10^{-4} of the incoming intensity, while the desired component has a transmission of approximately 0.96.

In operation, the polarizers have shown no tendency to damage. At 5kW input to each lamp, an output power of 600 watts has been observed in the main beam 82% vertically polarized. The secondary beam has been measured at up to 90 watts horizontally polarized and in operation is discarded. (See Figure 2-3). In practice a 12kW positive pulse having a rise time of 30ns and lasting for approximately 1 microsecond is applied. The first Pockels cell utilized a KD*P crystal immersed in trichloroethylene. The output pulses (see Figure 2-4) has a modulation superimposed on the main pulse and had an energy per pulse of 120mJ. The pulse widths were on the order of 30ns for a peak power on the order of 4MW. The repetition rate was increased to 600 pps at which point the fluid in the area of the beam and at the surface of the KD*P crystal began boiling. After replacing this fluid with a Dow Corning silicon oil (DC 200-5) and replacing windows the system operated well at up to 200 pps, however it was obvious that the fluid immersion technique would not be useful at high repetition rates due to heating. In addition it was found that the Pockels cell pulse electronics was inadequate in terms of pulse rise time, voltage capability and repetition rate since all three items degraded at repetition rates in excess of 800 pps.

In the course of measuring the pulse output characteristics it was realized that the modulation seen on the pulse was in fact quasi-self mode-locked with a natural frequency of 77 MHz which corresponds to the $c/2L$ mode of the laser system.



2.2 Mode-Locked Injection Technique

In order to obtain maximum second harmonic generation efficiency with the smallest possible crystal size it is desirable to increase the peak power output of the system to as high a level as possible. The technique which we have proposed and incorporated has demonstrated theoretically and experimentally that substantial increases in peak power can be achieved.

2.2.1 Mode-Locked Injection System Description

The peak power enhancement technique makes use of a continuous mode-locked Nd:YAG laser as a source of very short pulses which are injected into the cavity of the main high power laser, acting as seed pulses from which the Q-switched output can grow rather than from the natural laser fluorescence. The pulse injection is accomplished by sharing the output mirror of the CW mode-locked system with the front termination reflector for the main laser, as diagrammed in Figure 2-5.

A compromise reflectivity between the 90% optimum for the mode-locked system and 100% optimum for the main laser is utilized. With no voltage applied to the Pockels cell the horizontally polarized beam from the mode-locked system passes through the prism polarizer with a negligible portion (less than 1%) reflected into the high power system. In the ideal circumstance in which the Pockels cell is switched rapidly, in a time short compared with the time between mode-locked pulses, and with perfect synchronization one mode-locked pulse with a width of less than 200 picoseconds and an energy of approximately 3×10^{-8} joules is injected. If this amount of energy is adequate to completely dominate the natural fluorescence of the system, a condition which is met in practice, the final laser pulse will emerge with an energy essentially identical to that for the pure Q-switched condition but having the form of a pulse train consisting of narrow pulses separated in time by the round trip transit time of the main laser. An actual pulse photograph is shown in Figure 2-6. The envelope of this pulse train has a width approximately equal to the pure Q-switched pulse.

NOT REPRODUCIBLE

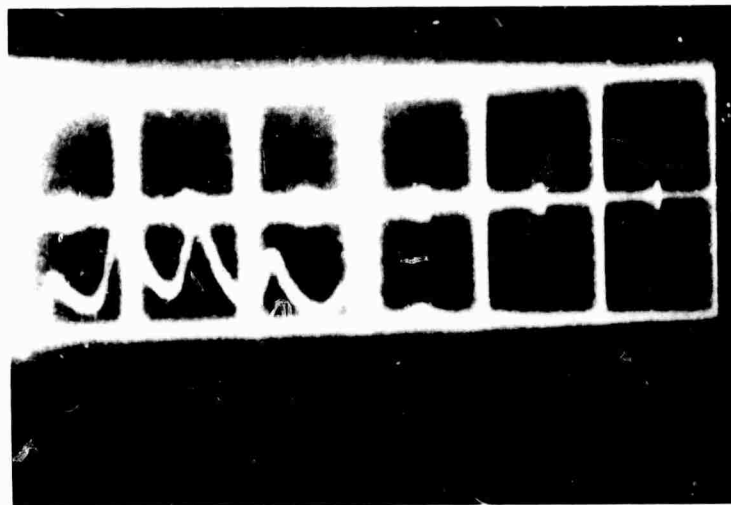


FIGURE 2-4

Single Trace of Q-Switched Output from Series
2500 8-Stage Laser System Showing Typical
Self-Mode-Locking Tendency at 77 MHz

Horizontal Scale - 20 nanoseconds/Division
Vertical Scale (approx.) - 5MW/Division
Total Energy = 150 Millijoules

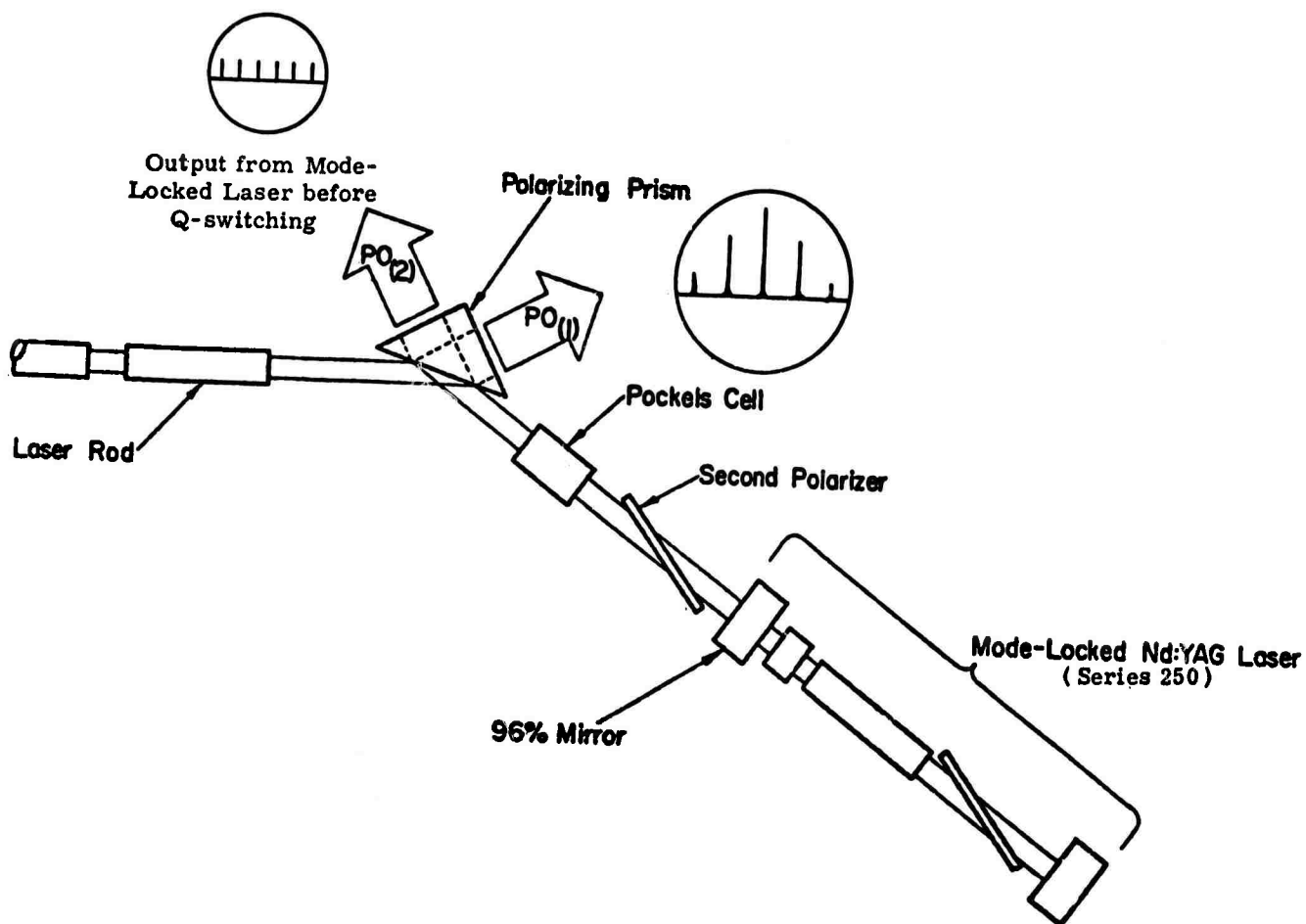


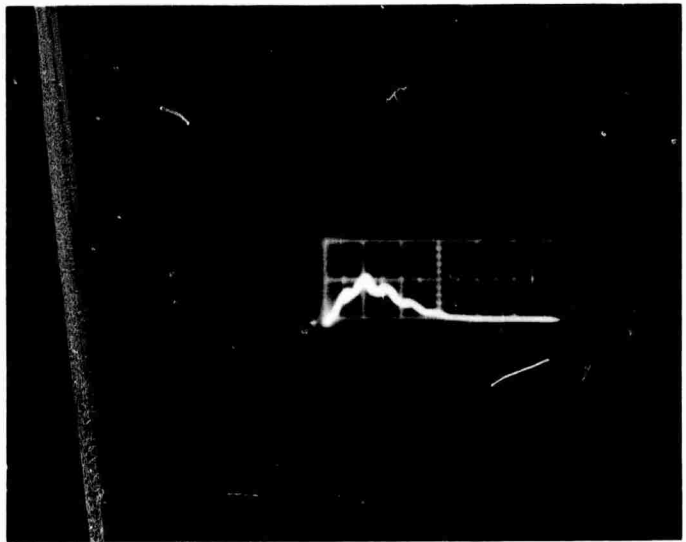
FIGURE 2-5

Detail Schematic of Series 250 Mode-Locked Laser
 Providing "SEED" Pulses to Series 2500 8-Stage
 Q-Switched Laser System



Neglecting saturation, the second harmonic generation process can be enhanced by factors of greater than 10 to 1 by this technique. Our system has demonstrated a 5 to 1 ratio, the discrepancy being due primarily to the imperfect electronic switching. In the implementation of this technique we have made use of both an open loop and a closed loop CW mode-locking system operating at 77 MHz, coincident with the round trip transit frequency of the main laser. The mode-locking system utilizes phase modulation, accomplished by means of a barium sodium niobate crystal, with electronics circuitry to provide closed-loop control of the modulator driving frequency so as to maintain perfect synchronization with the laser cavity frequency. A description of the closed loop mode-locking system developed independently by HoloBeam, Inc. can be found in the appendix.

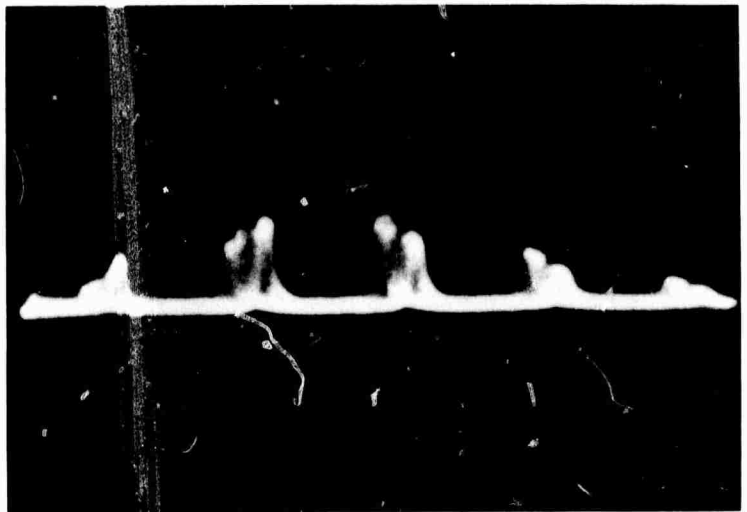
Horizontal Scale
20 N. S. / Div



"Q" Switched Only

NOT REPRODUCIBLE

Horizontal Scale
13 N. S. Between
Pulses



"Q" Switched and Mode Locked

FIGURE 2-6

Multiple Traces Showing Difference Between Normal "Q" Switched Output
and "Q" Switched with Open Loop Mode Locking Output at Equal Energy
Per Pulse



2.2.2 Experimental Results

The closed loop mode-locking electronics was completed and tests indicated that an output of 2 watts stably mode-locked at 77MHz could be obtained. The Series 250 complete mode-lock system was installed parallel to the Series 2500-8 stage laser according to the diagram in Figure 2-7. After resolving some coating problems with quartz windows obtained from Isomet Corp. a dry Pockels cell was designed and constructed utilizing highly deuterated KD*P obtained from Isomet since tests had shown this material could withstand in excess of 800 watts CW without overheating. In operation it was found that although there was some feedback from the Q-switched laser, the closed loop mode-lock system could mode-lock the Q-switched pulses reliably at repetition rates of up to 1000 pps. However the pulse energy fell off above 800 pps due to lower pulse voltages on the Pockels cell above that rate. The output energy per pulse was maintained at between 100 and 110 mJ (see Figure 2-8), however the pulse envelope width was somewhat longer during mode-lock operation possibly due to a slow rise time on the voltage pulse to the Pockels cell.

2.3 Switching Electronics

In order to produce optimum mode-locked pulse injection the Pockels cell should switch in a time short compared with the pulse-pulse separation and at a time accurately synchronized with the mode-locked pulse train. The thyatron pulses used in our initial experiments were borrowed from our low power CW laser system and had a switching time of approximately 30 nanoseconds. No synchronization was possible. In spite of this we could obtain stable mode-locked enhanced second harmonic generation. However, the observed 5:1 enhancement ratio was a factor of three worse than we should be able to achieve. We believe that this is due to incomplete injection, the mode-locked pulse being unable to dominate the fluorescence from the high power amplifier.

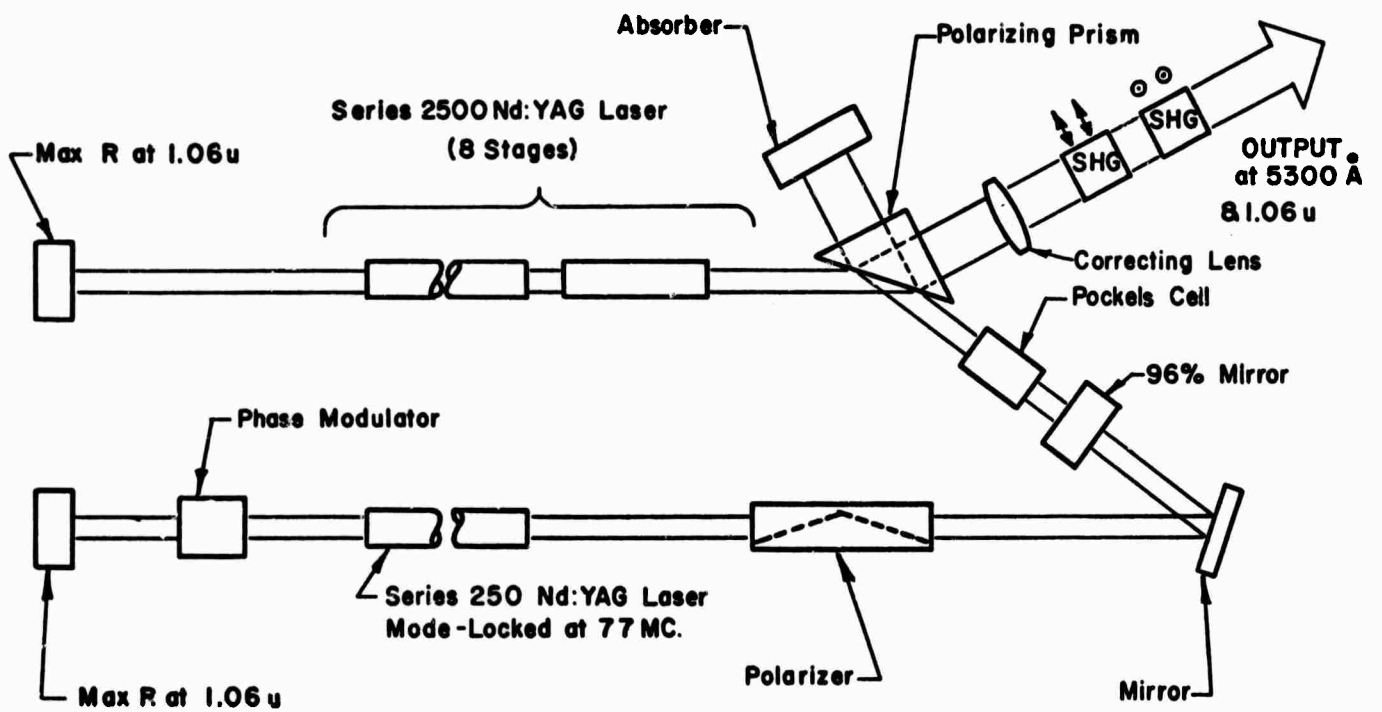
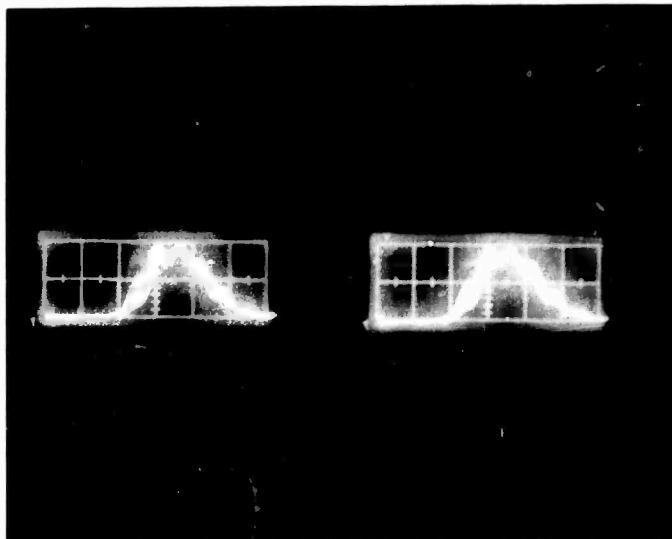


FIGURE 2-7

Detail Schematic of Complete Q-Switched and Mode-Locked and Frequency-Doubled Series 2500 8-Stage Laser System

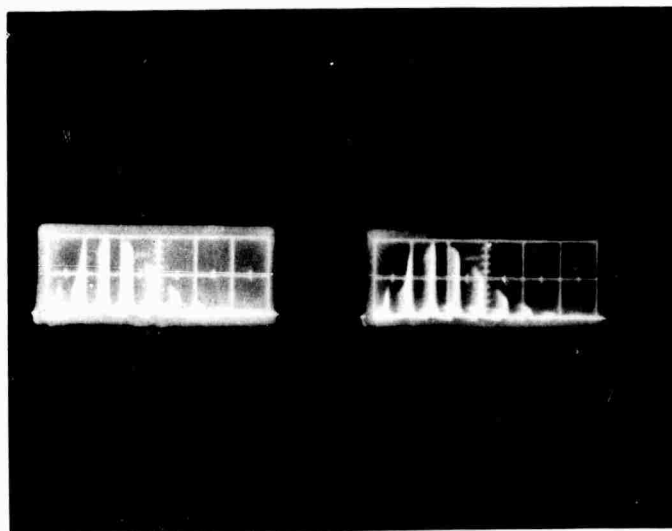
Horizontal Scale -
20ns/Div
Vertical Scale -
2.5MW/Div



Typical "Q" Switched Pulses at 1000 P. P. S.
and 110 Watts Average Output Power Utilizing
Holobeam Designed Dry Pockels Cell "Q" Switch

NOT REPRODUCIBLE

Horizontal Scale -
20ns/Div
Vertical Scale -
25MW/Div



Same as above when Closed Loop Mode-Locking
initiated

FIGURE 2-8

Oscilloscope Traces of Closed Loop Mode-Locked
"Q" Switched
Output at 110 M. J. /Pulse



SECTION III

NON-LINEAR MATERIALS

One of the major areas of concern in this program has been the selection and optimum utilization of a non-linear material which will yield high conversion efficiencies at high average powers from a multi-transverse mode laser.

3.1 Nonlinear Crystal Survey:

Since we recognized at the onset of the program that any non-linear crystal used to generate the 0.533 micron second harmonic of the 1.065 micron laser fundamental in Nd:YAG must be optically transparent at both wavelengths, many materials were precluded as primary candidates. As the program proceeded, only those non-linear crystals showing less than one percent absorption at 1.065 per centimeter were considered. Our own special technique for measuring 1.065 absorption (as described in paragraph 3.2) was utilized in making this selection. From materials so tested, only five major choices remained which showed less than $1. \% \text{ cm}^{-1}$. Since both peak and average power levels encountered by these crystals are highest at 1.065 microns, the selection of nonlinear materials for use in our experiments was predicated upon lowest absorption at that wavelength, with secondary emphasis placed upon their absorption at the second harmonic.

Listed below in Table I are the five materials which were given serious consideration in order of their degree of nonlinearity.



TABLE I
NONLINEAR CRYSTAL SELECTION

MATERIAL	POINT GROUP	LARGEST NONLINEAR COEFFICIENT*	PHASE-MATCH ANGLE AND TEMPERATURE
Ba ₂ Na Nb ₅ O ₁₅	mm2	$d_{32} = 41. \pm 4.$	90° @ 105°C
LiNbO ₃	3m	$d_{31} = 14. \pm 2.$	90° @ 165°C
LiIO ₃	6	$d_{31} = 11. \pm 2$	29°50' @ 25°C
KD ₂ PO ₄	42m	$d_{36} = 1.0 \pm 0.1$	39°57' @ 25°C
CsD ₂ AsO ₄	42m	$d_{36} = 0.55 \pm 0.05$ **	90° @ 101 °C

* Relative to d_{36} for KD₂PO₄

** Measured value may be in error due to improper crystal growth.



Thus far, CsD_2AsO_4 has given us the highest overall conversion of 1.065 micron output into average 0.533 micron second harmonic power in spite of the fact that it has the smallest degree of nonlinearity of all materials listed above. The two major factors which limit SHG conversion efficiency in $\text{Ba}_2\text{NaNb}_5\text{O}_{15}$ and LiNbO_3 are thermal runaway due to the poorly understood nonlinear heating effect at phase match, and the nonlinear catastrophic damage phenomenon, also poorly understood. Both LiIO_3 and KD_2PO_4 are limited by the large angular walkoff between the second harmonic and fundamental Poynting vectors, precluding the efficient use of long crystals. CsD_2AsO_4 is the only remaining choice which combines the advantage of 90-degree phase-matching angle and inherently greater angular acceptance with minimal self-heating due to nonlinear thermal effects. Curiously, at high power levels actual SHG conversion efficiencies observed in these materials have varied roughly inversely, rather than directly with the magnitude of their nonlinear coefficients.

3.2 Optical Absorption Measurement

In our past experience we have found very few optical materials that have withstood average 1.065 micron power densities beyond 25 kilowatts/cm² when placed in the high power output beam of our CW Nd:YAG system. Fused silica, undoped YAG and diamond are the only materials which have shown little or no lensing effect due to thermally-induced refractive index distortion at this wavelength. All other materials, including all nonlinear crystals tested, have shown significant thermal lensing. Therefore it became imperative to develop a technique for measuring relatively small residual absorption in nonlinear crystals, first to determine whether they would survive high average power levels at 1.065 microns, and secondly to aid in predicting the degree of phase mismatch resulting from thermally-induced nonuniformity across the input beam diameter. For this purpose we developed a successful technique based upon balancing the heat generated within a polished crystalline sample with a known amount of cooling developed by a Peltier junction device held in intimate contact with the crystal under



vacuum conditions such that no heat loss by convection took place.

The actual construction of the Peltier device is shown in the accompanying photograph, Figure 3-1 & 3-2. The base is machined from a special aluminum extrusion which clamps to our standard optical rail, and also serves as the hot junction heat sink for the Peltier cooler. The thermoelectric element itself consists of a doubly cascaded pair of semiconductor elements sandwiched between two aluminum plates and is configured to provide uniformity of temperature across the top cold junction plate. The unit was purchased from the Cambridge Thermionic Corporation as their Model 3955-1, which was selected for efficient operation at low current input levels, and because the top surface dimension of 1/2 inch coincided with the approximate side face dimensions of most crystals tested. The outer case is sealed with vacuum-tight fittings and incorporates an opposite pair of doubly antireflection-coated fused silica windows centered with respect to the axis of our Series 250 CW Nd:YAG system. A vacuum exhaust port permits hookup to a vacuum pump through a vacuum needle valve and liquid nitrogen cold trap. Additional vacuum sealed electrical feed through connections are provided to the Peltier cooler and to internal calibration terminals. A teflon shroud is placed beneath the top plate of the cooler for extra stray light shielding, and a gold-plated copper plate is placed atop the cooler to reflect away any spurious scattered light from the surfaces of the crystal under examination. A pair of Yellow Springs Instruments Corp. #44005 thermistor beads were used to record thermal equilibrium by inserting one at the top plate of the Peltier cooler in a drop of Wakefield Engineering Corp. zinc oxide impregnated silicone grease and the other into a hole drilled into the bottom aluminum block. A sensitive mercury battery driven Wheatstone bridge was used in conjunction with a Keithley Model 150B microvolt-ammeter to record null condition at room temperature.

A first trial run was conducted with a polished 1.0 cm^3 of best quality fused silica. A ten-watt 1.065 micron beam derived from a multimode CW Nd:YAG source was transmitted through

NOT REPRODUCIBLE

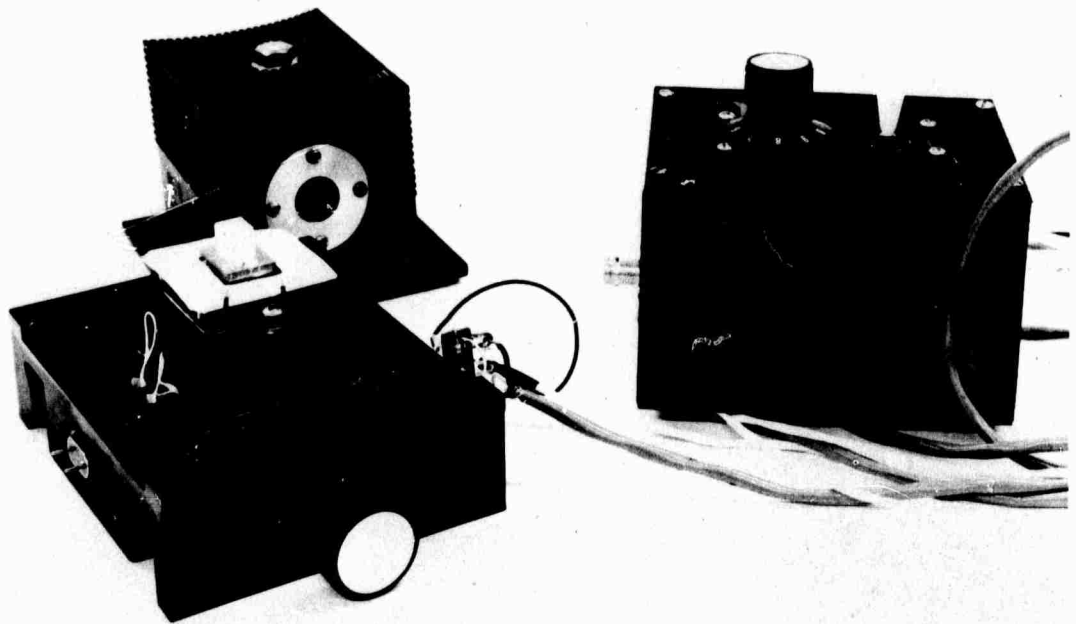


FIGURE 3-1

Construction of Peltier Device

NOT REPRODUCIBLE

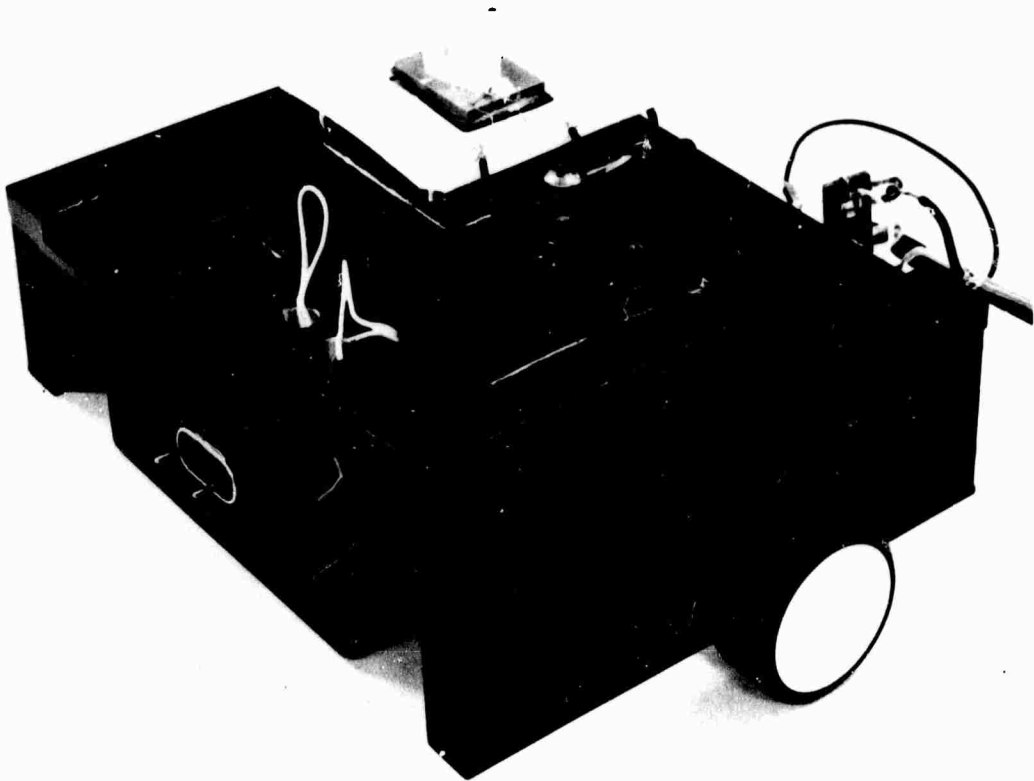


FIGURE 3-2

Closeup of Thermo-Electric Cooler Assembly



a 1.5 millimeter aperture stop, then through the Peltier cooler assembly evacuated to less than 10^{-5} mm. Hg., which contained the sample. The exit beam was captured by a Coherent Radiation Labs. Model 201 CW power meter, and the laser was adjusted to provide 10.0 watts. The Keithley microvolt-ammeter was quickly driven off-scale by absorption within the SiO_2 block. A small amount of current was then fed to the Peltier cooler to re-establish the previously set null point on the microvoltmeter. It was found that 3.6 milliamps of cooler current restored null, and that adequate sensitivity could be maintained at other laser power input settings using SiO_2 as a low absorption check.

A full calibration of the Peltier cooler under 10^{-5} mm Hg vacuum conditions was made utilizing a specially prepared aluminum block with a 100-ohm carbon resistor embedded within it. Heat, measured as the I^2R loss to the calibration resistor, was offset by the Peltier cooler current, and the calibration curves shown in Figure 3-3 were recorded for the three different Simpson milliammeter ranges used in later measurements. The shift in the curves for the ranges is caused by the difference in meter resistance.

Subsequent tests were performed on several specimens of nonlinear crystalline materials. Table II shows a complete list of test results obtained with a transmitted power at 1.065 microns of 10.0 watts under identical conditions. After each crystal was examined for its total heating effect upon the gold-plated copper plate, a teflon spacer ring was inserted under the crystal to thermally isolate it from the Peltier cooler. A second run was then made under vacuum conditions to ascertain what fraction of the total heating effect was due to combined internal Tyndal scattering and residual scattering from the polished crystal aperture faces. This contribution due to scattering was then subtracted from the original total heating term to yield a net figure for the absorption of a given length sample. The last column in Table II shows the renormalized absorption for each sample per centimeter length.

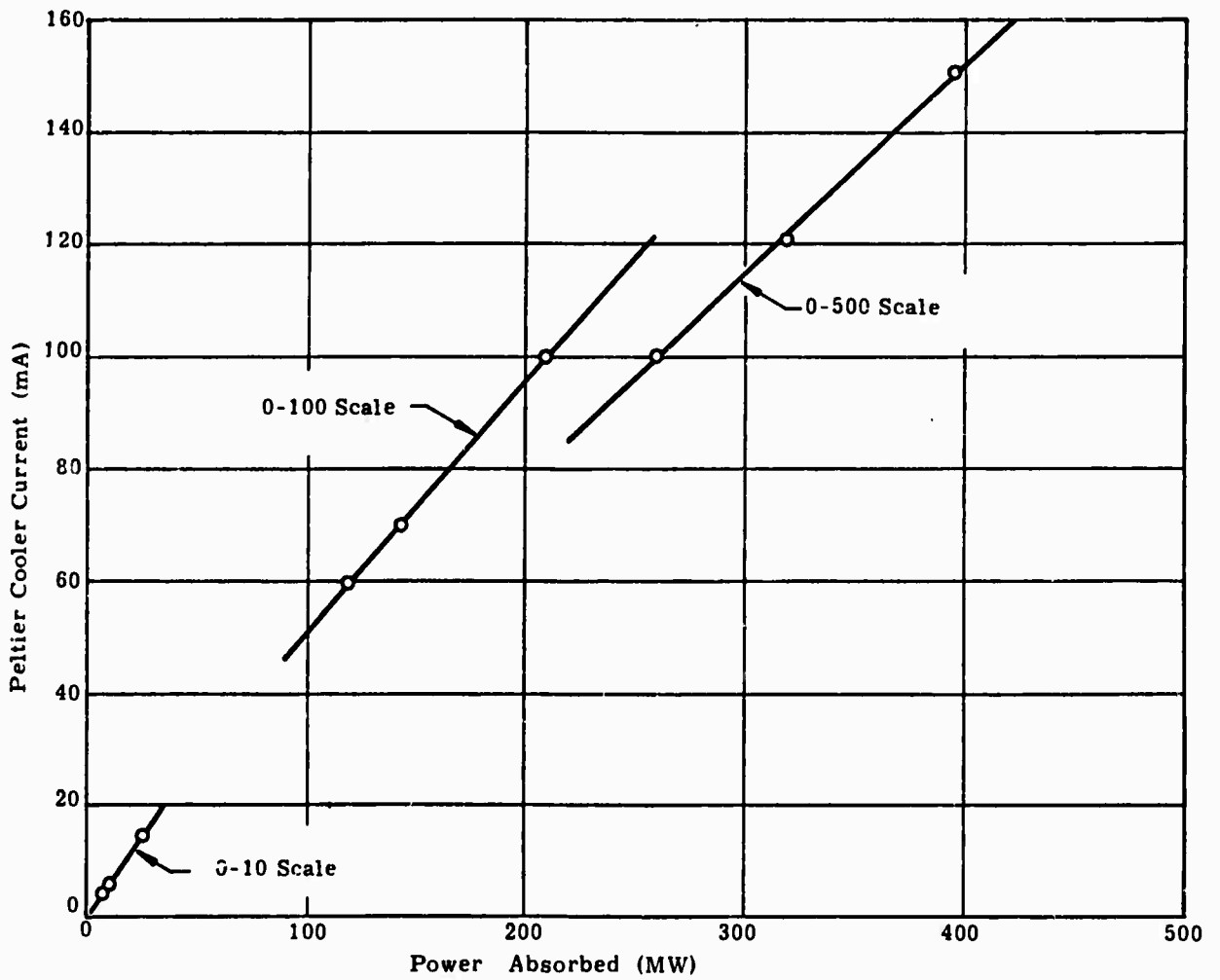


FIGURE 3-3

Peltier Cooler Calibration Curve



TABLE II
 PERCENTAGE ABSORPTION PER CENTIMETER OF LENGTH
 FOR NONLINEAR CRYSTAL SPECIMENS

Crystalline Material	Crystal Length (mm)	Null Current to Peltier Cooler, (10W Laser Input) (mA)	Cooling Power from Calib. Curve (mW)	Correction Due to Scattering (mW)	Adjusted Value for Absorption (mW)	Percentage Absorption per Centimeter crystal Length
CsD_2AsO_4	12.0	70.	155.	42.	113.	0.94
CsD_2AsO_4	10.0	60.	134.	36.	98.	0.98
CsH_2AsO_4	15.5	225.	610.	50.	560.	3.6
CsH_2AsO_4	15.5	215.	580.	50.	530.	3.4
KD_2PO_4	12.5	38.	95.	11.	84.	0.67
KD_2PO_4	12.5	41.	98.	11.	87.	0.70
KD_2PO_4	19.2	41.	98.	10.	88.	0.46
LiIO_3	5.0	6.5	11.	1.	10.	0.20
KH_2PO_4	14.0	450.	1040.	62.	978.	7.0
$\text{Ba}_2\text{NaNb}_5\text{O}_{15}$	5.0	9.3	16.0	1.	15.0	0.30
$\text{Ba}_2\text{NaNb}_5\text{O}_{15}$	5.0	8.9	15.4	1.	14.4	0.29
SiO_2 Block (as reference)	10.0	3.6	6.1	- - -	6.1	0.06



TABLE III
AVERAGED PERCENTAGE ABSORPTION FOR
NONLINEAR CRYSTALS TESTED.

Crystalline Material	Chemical Symbol	Measured Average Absorption per Centimeter
Lithium Iodate	LiIO_3	0.0020 ± 0.0001
Barium Sodium Niobate	$\text{Ba}_2\text{NaNb}_5\text{O}_{15}$	0.0030 ± 0.0001
Deuterated KD*P	KD_2PO_4	0.0061 ± 0.0012
Deuterated CD*A	CsD_2AsO_4	0.0096 ± 0.0002
Ordinary CDA	CsH_2AsO_4	0.035 ± 0.001
Ordinary KDP	KH_2PO_4	0.070 ± 0.002
Fused Silica (as reference)	SiO_2	0.0006 ± 0.0001



Table III is a consolidated listing of percentage absorption per centimeter length averaged over one or more measured specimens for each nonlinear crystal tested. With the exception of KD_2PO_4 , the average deviation from one sample to another was relatively small. The one sample of KD_2PO_4 which showed significantly lower absorption came from a different vendor than the others and is believed to be of higher deuteration.

3.2.1 Transmission Data

We have taken spectrophotometer tracings of CD*A and KD*P. These are shown in Figure 3-4.

Note that the CD*A sample has a measureably larger absorption at 0.355μ (third harmonic of 1.065μ).

3.3 Phase-Match Temperature and Efficiency of the Arsenates

A pulsed Nd:YAG laser was utilized to roughly measure the phase-match temperature and obtain an approximate efficiency. It was also desirable to determine, if possible, a damage threshold level for CDA and CD*A in terms of power density. The laser initially used was a 10 pps 3mm diameter system capable of 3MW peak power. It was found that the phase-match temperature for the initial samples of CD*A was around 97° and very broad — on the order of $+3^\circ\text{C}$. The efficiency for a power density of $50\text{MW}/\text{cm}^2$ was $\bar{12}\%$. The phase-match temperature for CDA was found to be 39.9°C and more critical than in CD*A. The efficiency was essentially the same as CD*A. Since no damage occurred to either crystal it was decided to increase the power density by utilizing a different pulsed YAG laser. This system was capable of an output of 180 mJ/pulse operating at up to 5 pps and had a peak power of 20MW in a 5mm diameter beam. For comparison purposes a 2cm long KD*P crystal cut for angular phase matching was utilized for SHG. At a power density of $80\text{mW}/\text{cm}^2$ the KD*P produced an efficiency of 5.4% (beam divergence was on the order of 4mR). At the same power density a 1 cm long CDA crystal was found to have an efficiency of 16% at phase-match temperature. No damage occurred to the crystal so

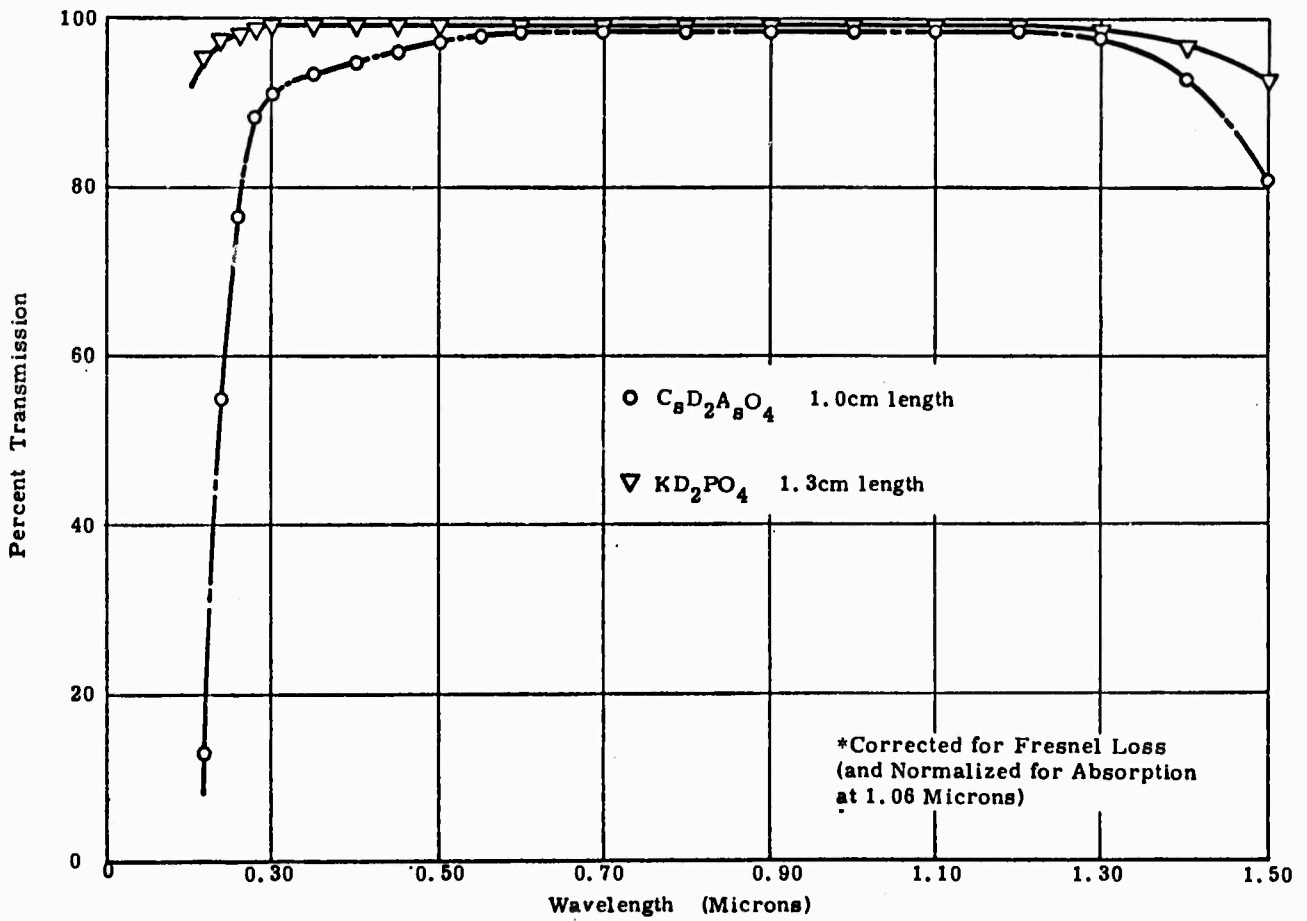


FIGURE 3-4

Transmission Curves for Deuterated Crystals*



the power density was increased by weakly focusing the beam to a diameter of 3mm, yielding a power density of $280\text{MW}/\text{cm}^2$. No damage occurred with the 1.06 micron radiation alone. See Figure 3-5. At phase-match temperature the efficiency increased to 30%. After operating for several minutes at 5pps it was found the fluid used in the cell (DC 200-5) was breaking down but no damage was seen on the CDA crystal, therefore it is concluded that the damage threshold for CDA is in excess of $300\text{mW}/\text{cm}^2$.

3.4 CsD₂AsO₄ Temperature Phase-Matching

Figure 3-6 is a photograph of the oven configuration used to accurately determine the phase-matching characteristics of CsD₂AsO₄ versus temperature. The inner split block was machined from a copper rod of approximately 460 grams mass, and provides uniform heating of frequencydoubling crystals 1.0 centimeter cube in size. A 70-ohm heater winding is situated in the outer housing wound around a copper tube which transmits heat uniformly to the inner copper block. Sufficient teflon insulation is provided between the heater and the outer oven housing to form an adiabatic jacket surrounding the entire copper interior. Doubly antireflection coated fused silica windows are positioned in air-tight seals at each end of the oven assembly. Electrical heating is provided from an automatically proportioning magnetic amplifier which senses the central oven temperature by means of an iron-constantan probe inserted into the split copper block. The overall rate of heating and the maximum oven temperature can be adjusted by proper selection of series ballast resistance.

Figure 3-7 is an actual trace of the temperature phase-matching profile for a 10.5 millimeter length of CsD₂AsO₄ cut for 90-degree phase matching with the input laser signal propagating parallel to the crystalline (110) direction. The trace was produced

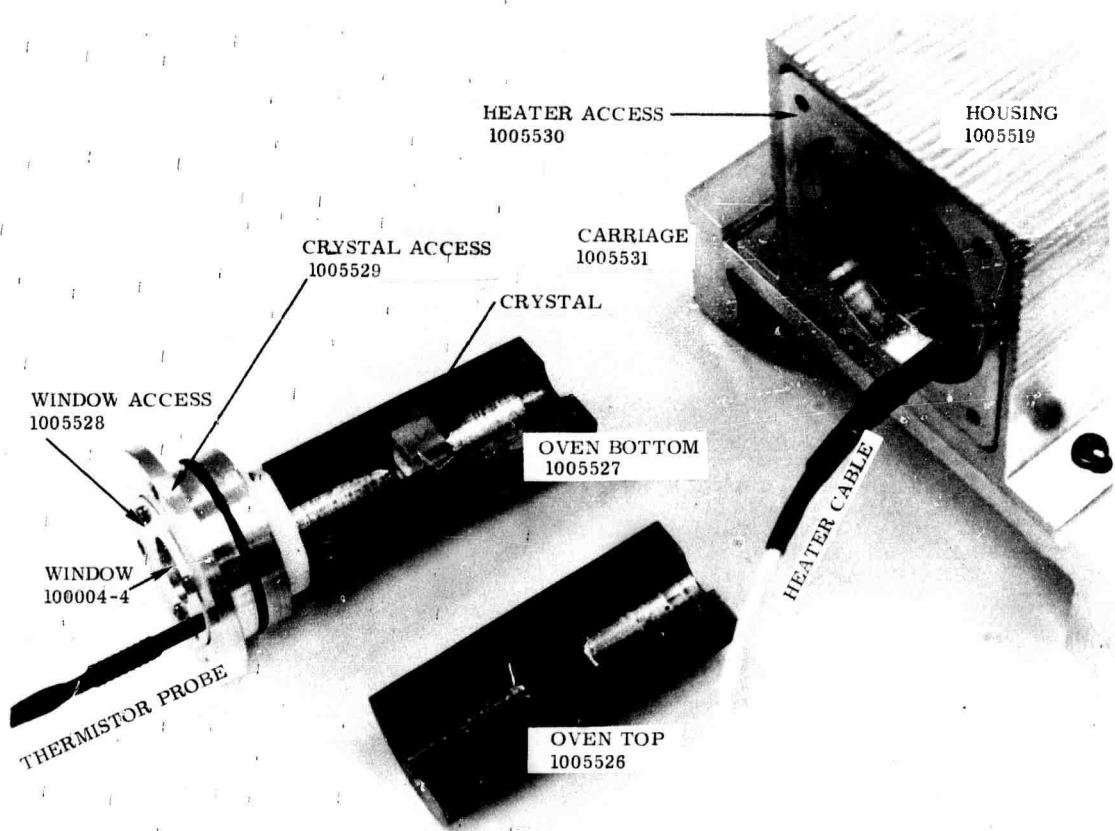


FIGURE 3-6

Oven Assembly for Testing Phase-Match Temperature
of 90° Phase-Matchable SHG Materials



the power density was increased by weakly focusing the beam to a diameter of 3mm, yielding a power density of $280\text{MW}/\text{cm}^2$. No damage occurred with the 1.06 micron radiation alone. See Figure 3-5. At phase-match temperature the efficiency increased to 30%. After operating for several minutes at 5pps it was found the fluid used in the cell (DC 200-5) was breaking down but no damage was seen on the CDA crystal, therefore it is concluded that the damage threshold for CDA is in excess of $300\text{mW}/\text{cm}^2$.

3.4 CsD₂AsO₄ Temperature Phase-Matching

Figure 3-6 is a photograph of the oven configuration used to accurately determine the phase-matching characteristics of CsD₂AsO₄ versus temperature. The inner split block was machined from a copper rod of approximately 460 grams mass, and provides uniform heating of frequencydoubling crystals 1.0 centimeter cube in size. A 70-ohm heater winding is situated in the outer housing wound around a copper tube which transmits heat uniformly to the inner copper block. Sufficient teflon insulation is provided between the heater and the outer oven housing to form an adiabatic jacket surrounding the entire copper interior. Doubly antireflection coated fused silica windows are positioned in air-tight seals at each end of the oven assembly. Electrical heating is provided from an automatically proportioning magnetic amplifier which senses the central oven temperature by means of an iron-constantan probe inserted into the split copper block. The overall rate of heating and the maximum oven temperature can be adjusted by proper selection of series ballast resistance.

Figure 3-7 is an actual trace of the temperature phase-matching profile for a 10.5 millimeter length of CsD₂AsO₄ cut for 90-degree phase matching with the input laser signal propagating parallel to the crystalline (110) direction. The trace was produced

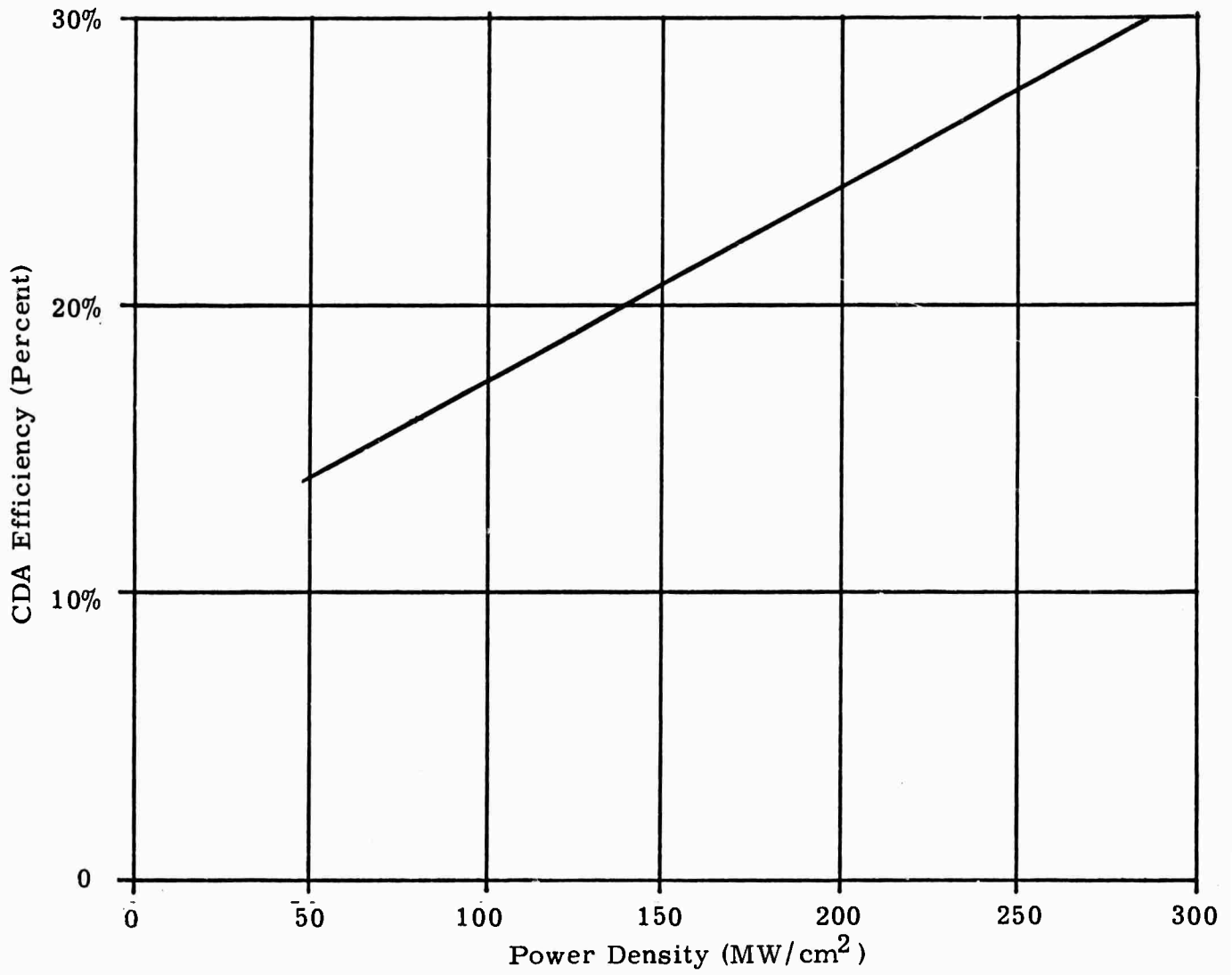


FIGURE 3-5

CDA Efficiency versus Power Density for Pulsed Operation

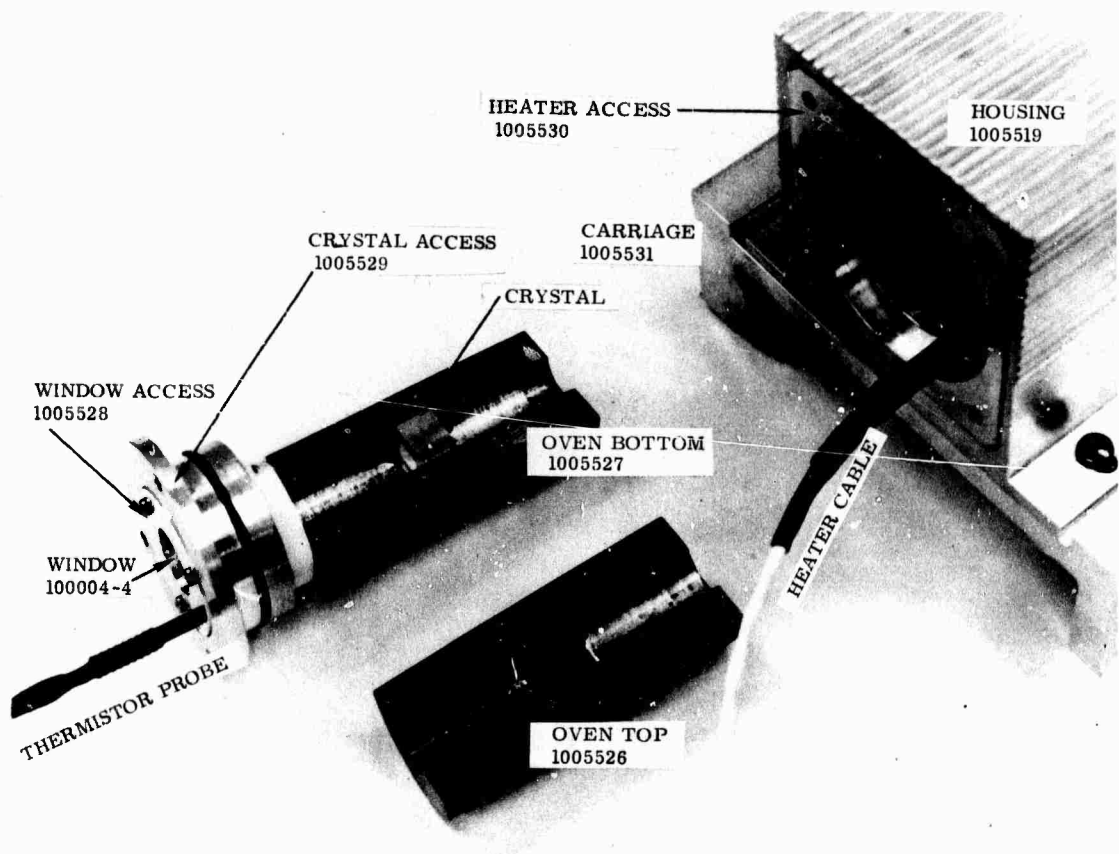


FIGURE 3-6

Oven Assembly for Testing Phase-Match Temperature
of 90° Phase-Matchable SHG Materials



by first allowing the oven temperature to exceed 130°C , then turning off heater power and letting the crystal slowly cool through its $\sin^2 \frac{(\Delta k l)}{2} / \frac{(\Delta k l)}{2}$ maxima and minima while

subjected to a half-watt, linearly polarized TEM₀₀ input beam from a CW Nd:YAG laser. An S-4 cathode photomultiplier was provided with a narrow bandpass filter peaked at 0.533 microns, and its anode current fed to a fixed load resistance across the Y-channel input to an X-Y recorder. The X-channel was used to monitor temperature by the output from a microvoltmeter connected directly to the iron-constantan thermocouple imbedded in the crystal oven. Only a coarse adjustment of CsD₂AsO₄ crystal angle was required with respect to the input laser beam since its angular insensitivity had been verified earlier.

The resultant curve in Figure 3-7 indicates that the CsD₂AsO₄ sample tested has a central peak situated at 101°C , with a half SHG maximum bandwidth, $\Delta T_{1/2}$, equal to 5.6°C . Both the position of the central maximum with respect to temperature and the half-power temperature bandwidth are strongly dependent upon the level of deuteration for a given CsD₂AsO₄ sample. It is therefore very important to run an individual check of both these factors for each delivered specimen, especially if two or more crystals are to be used in a tandem frequency doubling arrangement. Conversely, these factors can be utilized as criteria for judging the level of deuteration, which shifts the temperature peak, and the degree of crystalline homogeneity, which should prove directly related to the half-SHG-power temperature bandwidth for a given length sample.

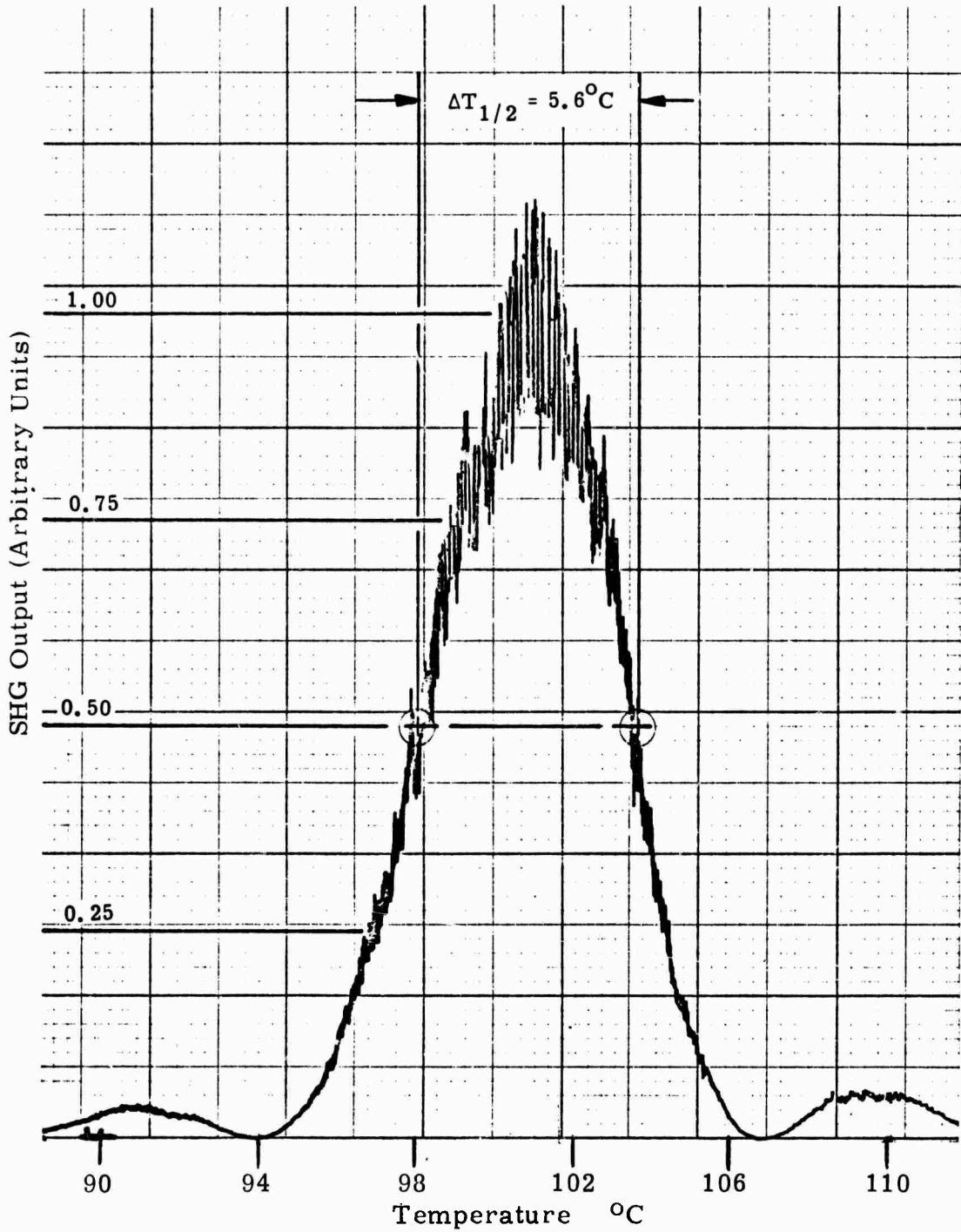


FIGURE 3-7

CsD_2AsO_4 Phase-Match Versus Temperature



SECTION IV

SECOND HARMONIC GENERATION AT HIGH AVERAGE POWER

We will first present the experimental evidence in chronological sequence and then discuss the implications of the data with respect to theoretical predictions.

4.1 SHG Apparatus and Tests

The complete system at the end of the development program is shown in Figures 4-1 thru 4-6. The SHG oven shown in Figure 4-7 and situated outside the laser cavity is also a vacuum chamber since the CD*A material is very hygroscopic and must be protected against water or water vapor. Two ovens are enclosed in the same chamber since it was expected that multiple crystals would be utilized to obtain maximum output at 0.53μ . The first test at full power allowed only the central portion of the beam to be incident upon the CD*A crystal at a power density of approximately $5\text{MW}/\text{cm}^2$ without mode-locking. The mode-locking injection increases this power density; however, the improvement in peak amplitude is unknown at this time since it has not been possible to measure the mode-locked pulse widths accurately. The output at 0.53μ was between 10 and 20 milliwatts with a 5 watt average 1.06 micron input at 100 pps. The mode-locking enhancement of the green was approximately a factor of 3.

4.1.1 SHG with Barium Sodium Niobate

At this point in time it was decided to attempt to determine if another SHG material might be usable. The highest theoretically efficient material obtainable at this time is barium sodium niobate which has been shown to damage at power densities of only 1 or $2\text{mW}/\text{cm}^2$ when phase matched and producing SHG. Accordingly, a crystal of this material was placed in the chamber in place of the CD*A. The first crystal chosen was a thin section that had been used on another program and was of extremely poor quality and otherwise unusable. The power density was slowly increased at a low repetition rate and at phase-match temperature, to the same level used on the CD*A. No damage occurred and the total green output was on the order of 100 mW. Since no damage occurred it was decided that a high quality barium sodium crystal should be

NOT REPRODUCIBLE

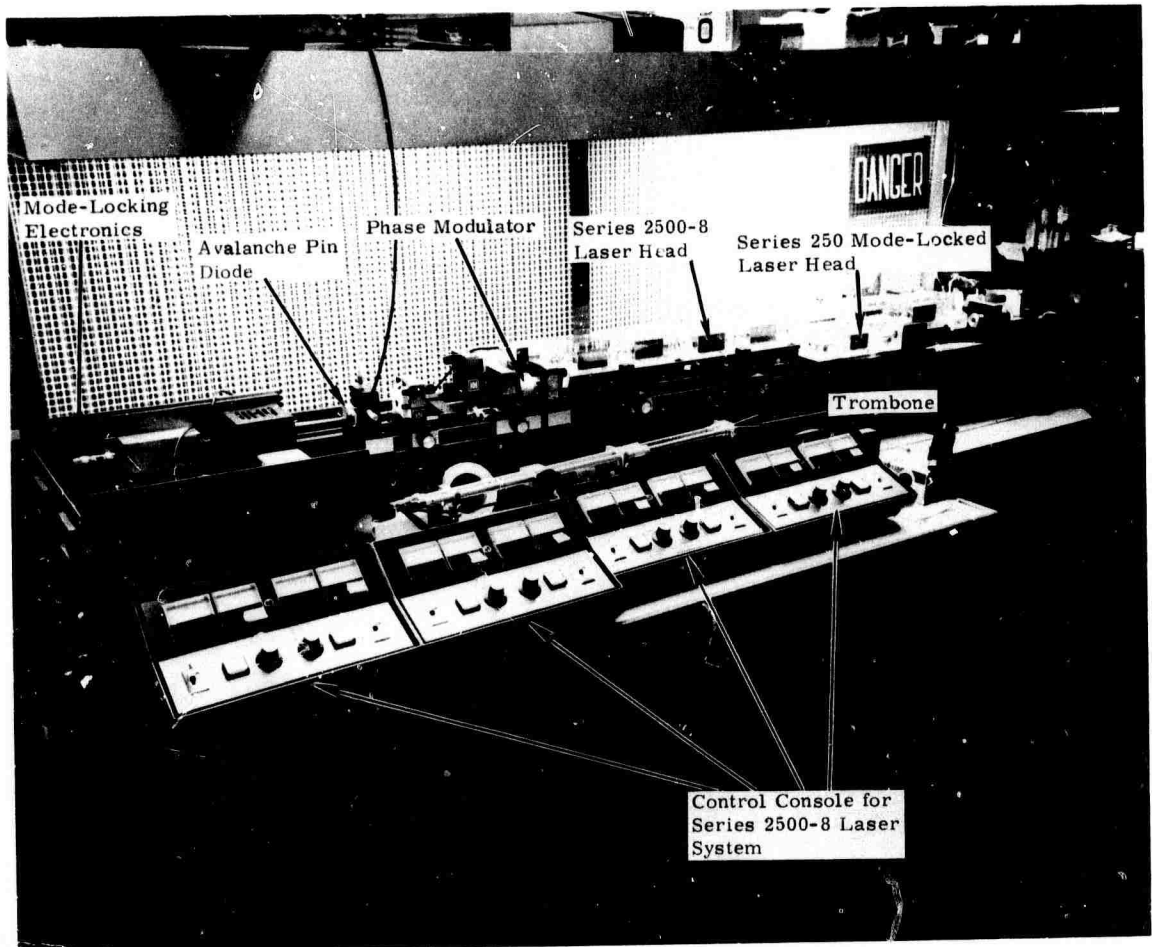


FIGURE 4-1

Experimental Arrangement of Complete System

NOT REPRODUCIBLE

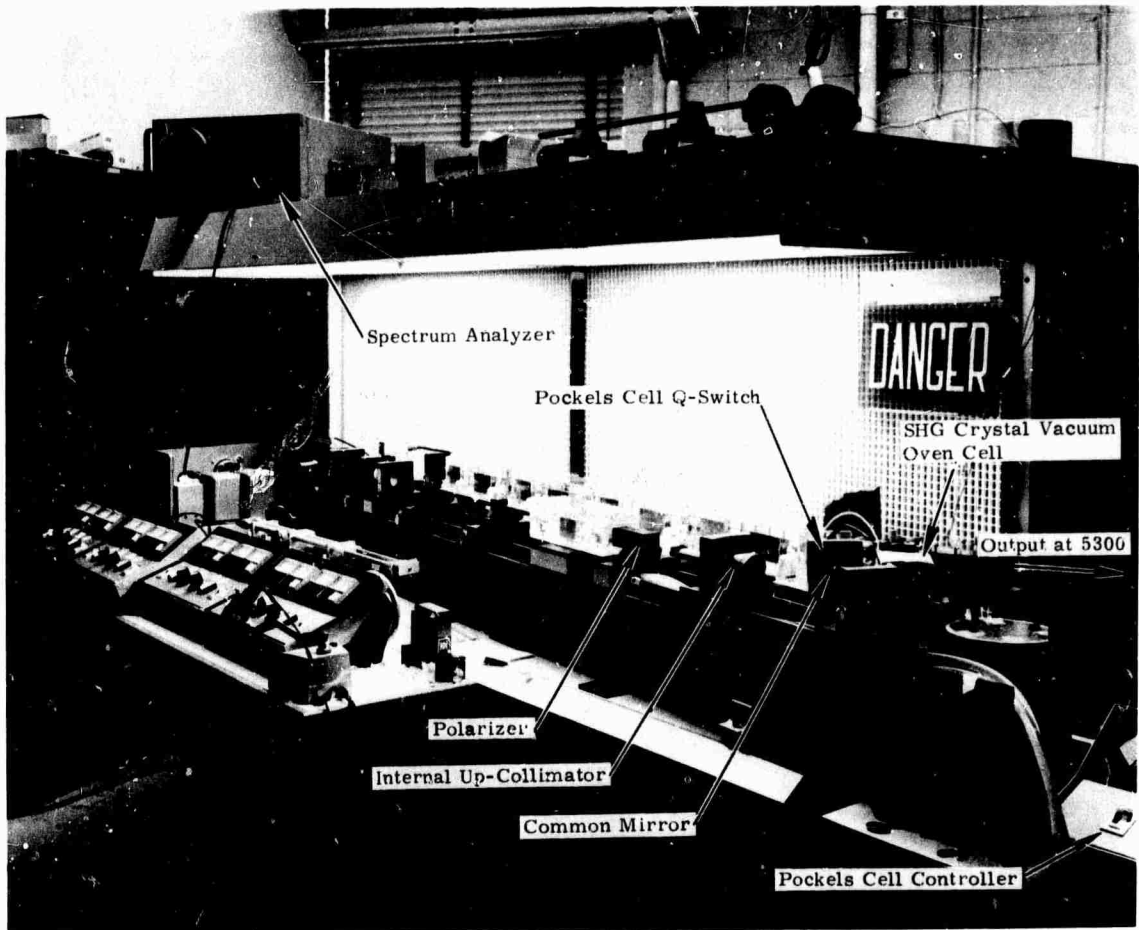


FIGURE 4-2

Experimental Arrangement of Complete System

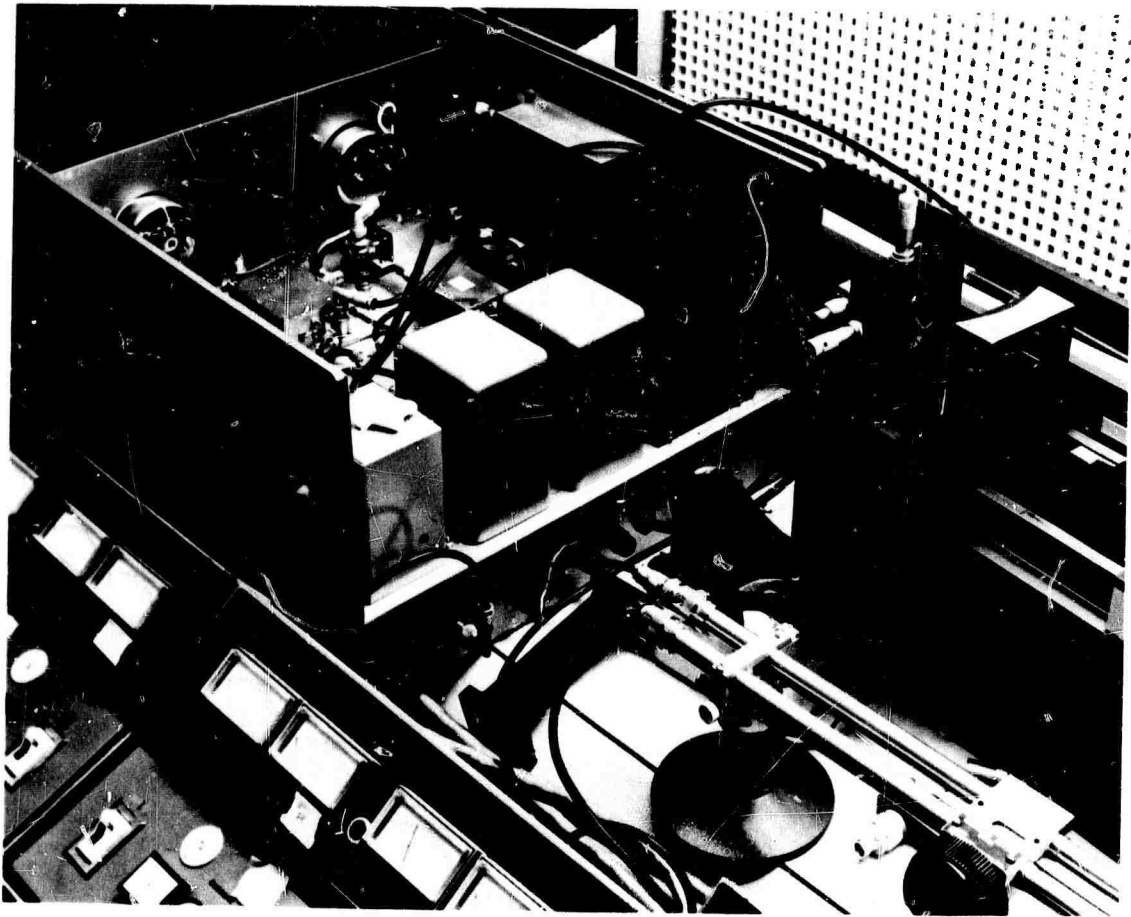


FIGURE 4-3

Mode-Locking Electronics for 77MHz

NOT REPRODUCIBLE

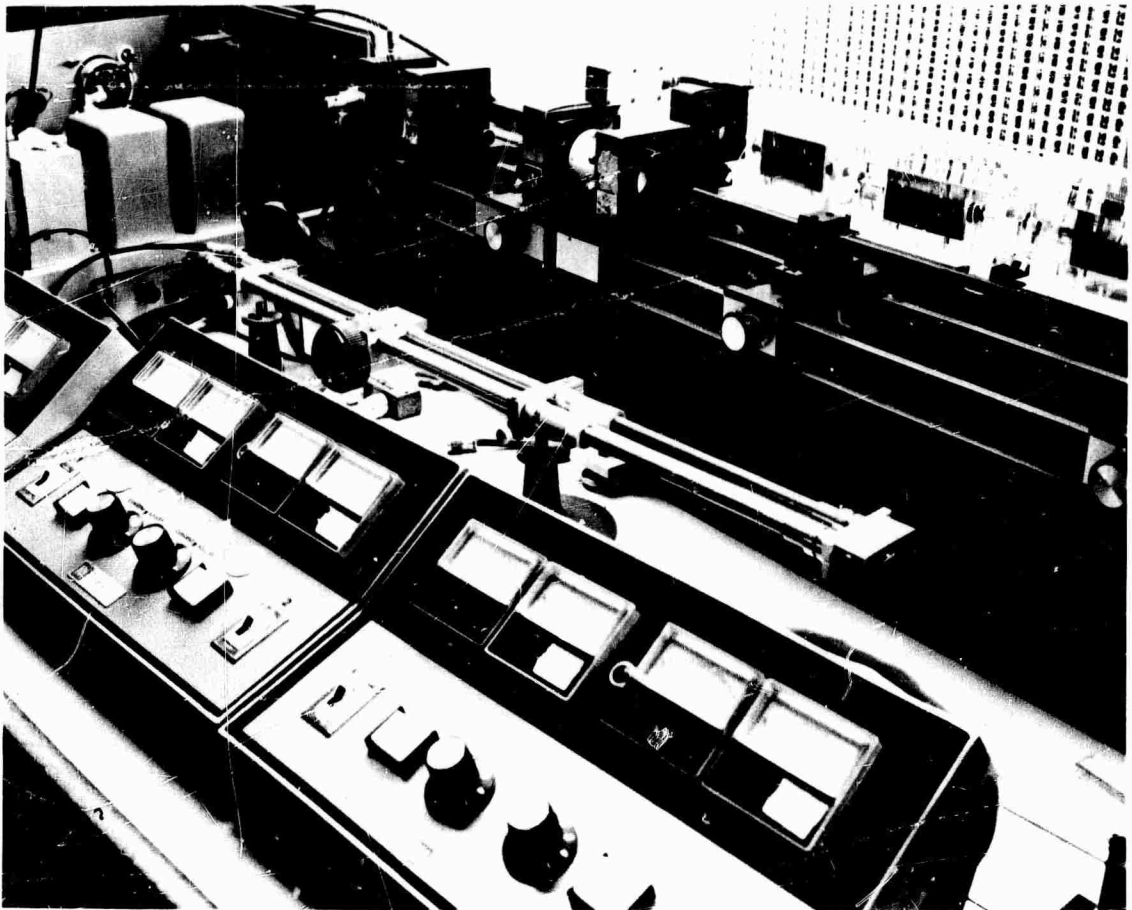


FIGURE 4-4

Variable "Trombone" for Phase Control of 77MHz R. F. Signal

NOT REPRODUCIBLE

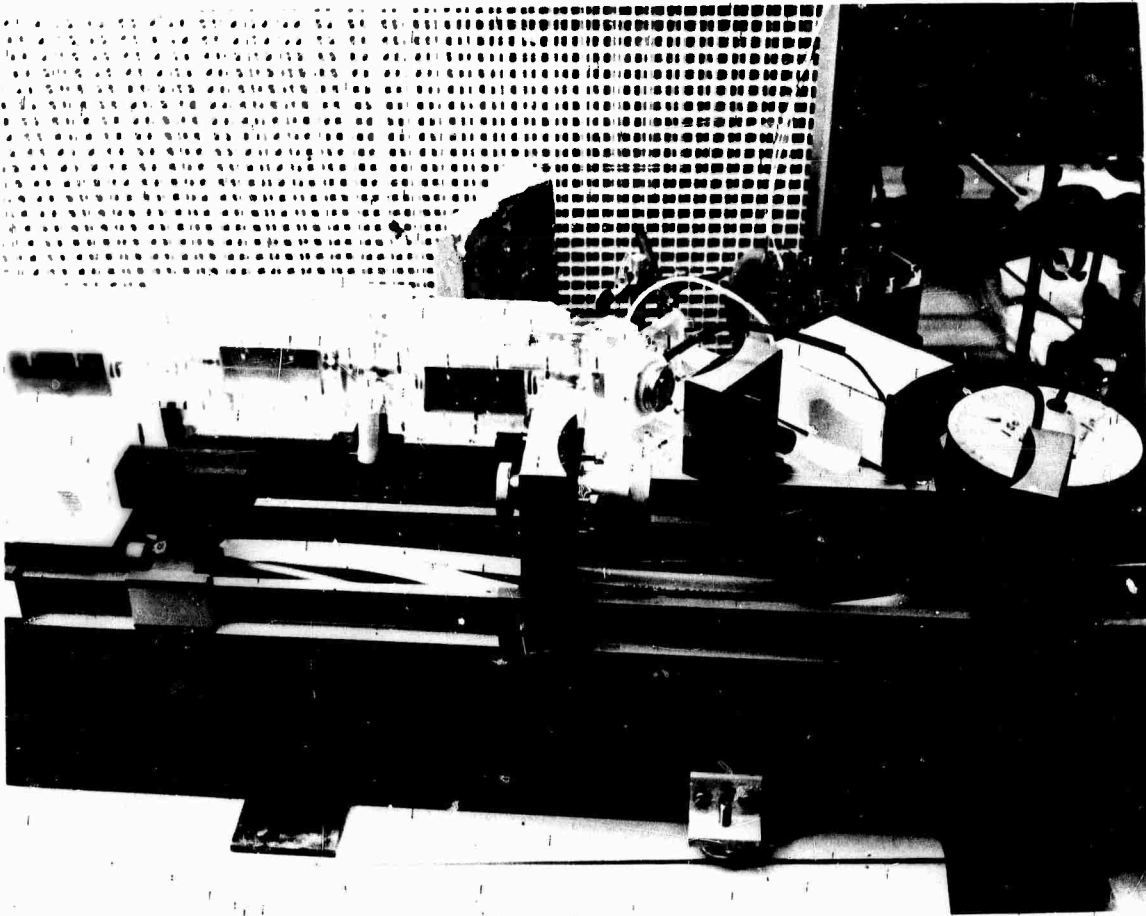


FIGURE 4-5

Series 250 Mode-Locked (Foreground)
Pulse Injection and "Q" Switch Pockels Cell
Integration Mechanism (Center-Right) and
Series 2500-8 Laser (Background)

NOT REPRODUCIBLE

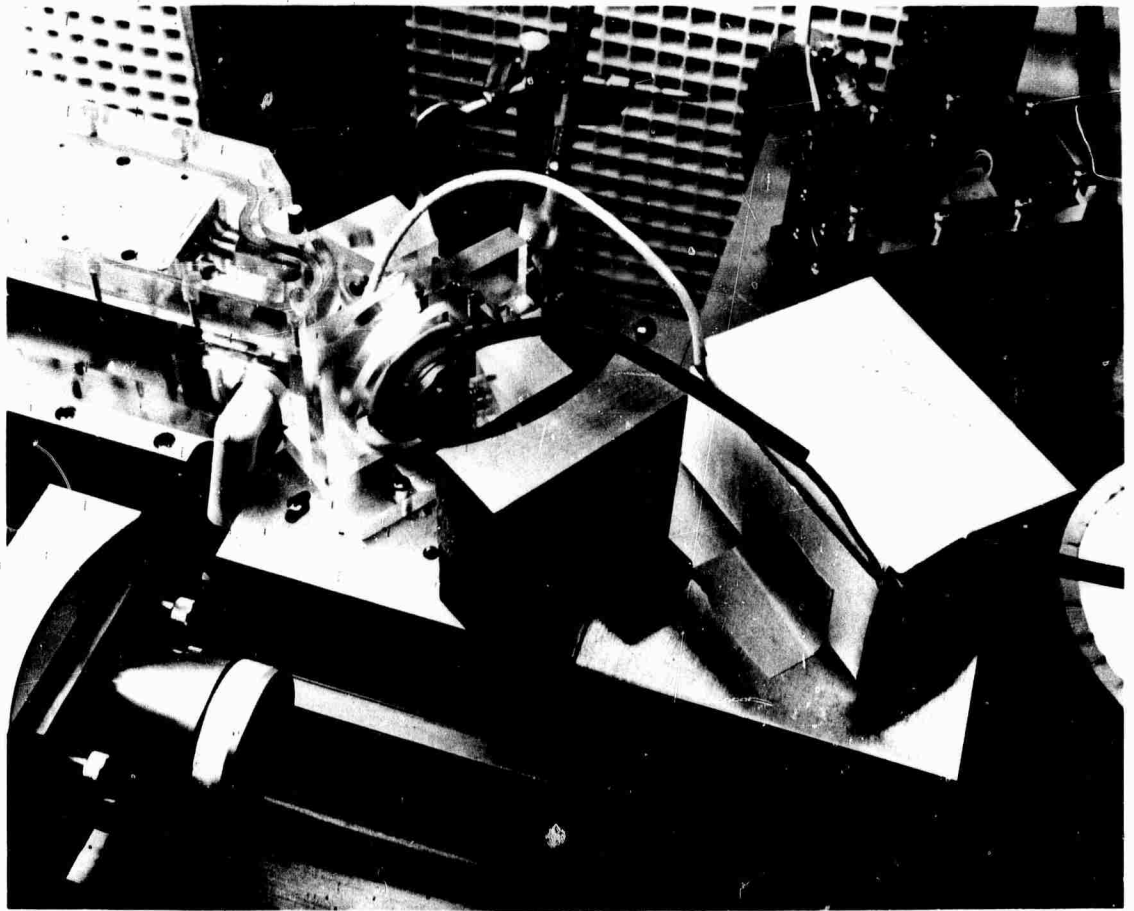


FIGURE 4-6

"Q" Switch Pockels Cell Assembly in Position
Between Last Stage of Series 2500-8 Laser and
Mirror Command with the Series 250 Mode-Locked Laser.
Output of System is to the Upper Right Side

NOT REPRODUCIBLE

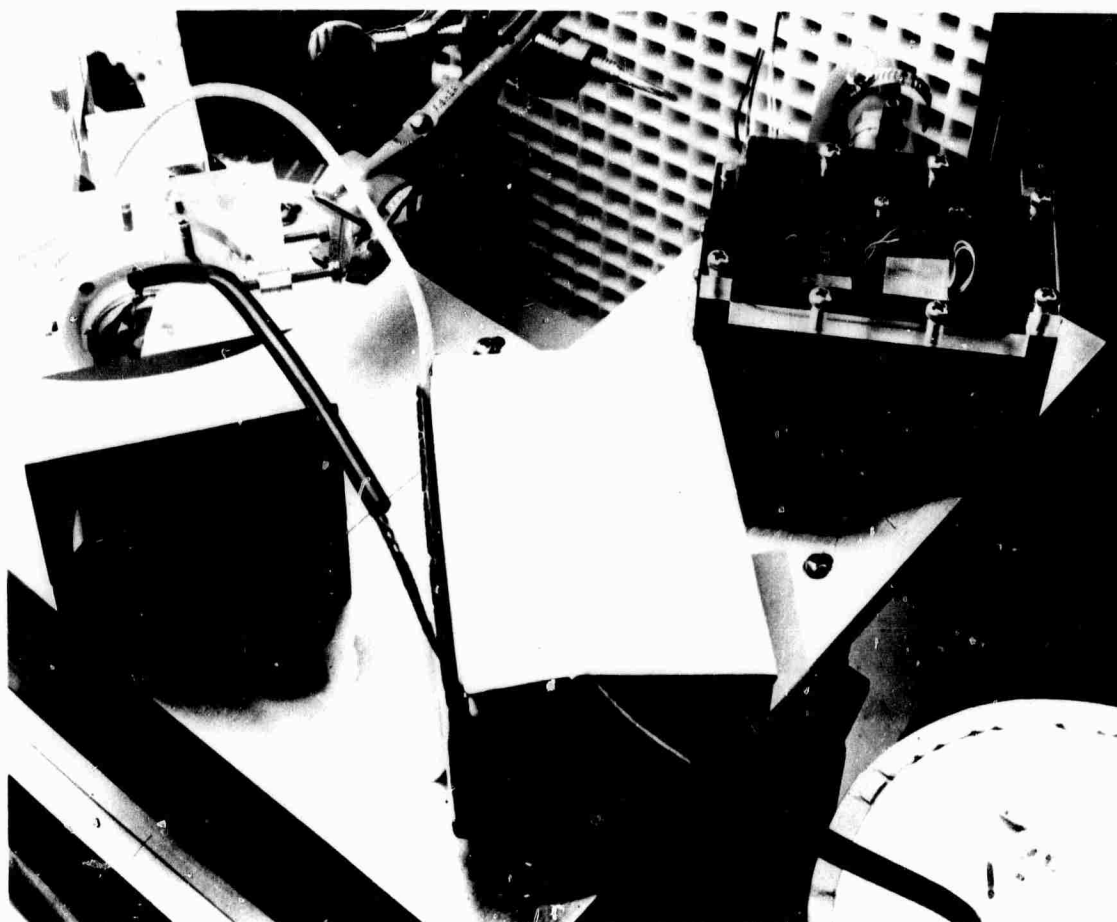


FIGURE 4-7

Output of Laser System is Through Lens at Upper Left
then Through Frequency Doubling Over/Cell Windows
and SHG Material (Upper Right)



risked. Such a crystal was installed in the oven. At full power in (the beam was apertured to 3/16 inch diameter to fill the crystal) the total average power at 1.06 μ passing through the crystal was 6 watts at 100 pps. At phase-match temperature (92°C) the output was 0.7 watts at 0.53 μ without mode-locking. When the mode-locked pulses were allowed to dominate the Q-switched pulse the green output decreased to approximately 0.3 watts immediately. To check this effect the temperature of the crystal was taken well above the phase-match point (to 125°C) and the mode-locking would indeed enhance the output by a factor of 2 to 3. As the temperature on the crystal was allowed to decrease toward phase match, the mode-locking was turned off and on intermittently showing a decrease in SHG enhancement as phase-match was approached. At an average output (at 100 pps) of 300 mW the mode-locking became ineffective. As the mode-locking was introduced a decrease in 1.06 micron power was noted with no corresponding increase at 0.53 μ . (Both the 1.06 micron output and the 0.53 μ output were being monitored separately.) As the temperature on the crystal was allowed to decrease further toward phase-match an instantaneous decrease in SHG output would be seen as mode-locking was introduced; then a further decrease would occur as the temperature on the crystal increased further away from phase-match temperature. At the moment the mode-locking was introduced, a corresponding decrease of power would also occur in the 1.06 micron beam passing through the crystal. In other words, power was being lost by some mechanism inside the barium sodium niobate crystal. At phase-match temperature the unmode-locked average output was 0.7 watts and the 1.06 micron average output was 4.5 watts (normal output without SHG was 5.2 watts average). When mode-locking was introduced this output fell to approximately 3.8 watts. Therefore a power of 0.4 watts (at 0.53 μ) plus 0.7 watts (at 1.06 microns) or a total power of 1.1 watts was being lost by some unknown mechanism. It was obvious that this power was being absorbed by the barium sodium niobate crystal since the temperature in the crystal would increase dramatically. To maintain a temperature just above phase-match it was necessary to remove all heating current from the oven. The heating from the absorption process was sufficient to maintain phase-match temperature for 5 to 10 minutes. Eventually, however, the temperature would finally fall just below phase-match and would then fall very rapidly thereafter. If the crystal temperature were increased from below phase-match temperature, as phase-match was approached a thermal runaway would occur taking the crystal temperature



through phase match and then well beyond. This phenomenon has been noted before and is usually referred to as a temperature hangup at phase-match and has been attributed to an absorption at 0.53μ . These tests however, clearly show that it is not associated with absorption at 0.53μ since this would not account for the instantaneous decrease in 5300°A output when mode-locking is introduced. Instead it appears that it may be due to a two-photon process causing an absorption at an equivalent of 0.355μ since barium sodium niobate does have an absorption edge in the near ultra violet. This phenomenon may in fact explain why this material damages at low power densities when phase-matched and the 1.06 micron beam is small in diameter. However, in vivid contrast to earlier experiments in CW second harmonic generation, no surface damage occurred in these tests with a relatively large beam. However an internal damage spot did appear in the form of a series of tiny bubbles, all in a single plane set at approximately 30° to the optical axis. No further tests were performed with barium sodium niobate.

4.1.2 SHG with Lithium Niobate

In an effort to determine if the same effect just described is prevalent in other materials, a crystal of lithium niobate was inserted into the oven in place of the barium sodium niobate. At the same power density and repetition rate as used in the previous test, the lithium niobate produced an output of 0.8 watts average at 0.53μ with mode-locking and 0.3 watts without mode-locking at phase-match temperature (about 200°C). However by carefully measuring the 1.06 micron output and the 0.53μ output at phase match approximately 0.2 watts of power were missing, presumably absorbed by the lithium niobate by the same or a similar mechanism as in barium sodium niobate. In addition, the same effect of "hanging up" in temperature as the temperature is lowered past phase-match was observed as well as a thermal runaway in approaching the phase-match temperature from below phase match. However the effect was far less severe than in "banana". The power density was subsequently increased in the lithium niobate by lightly focusing the beam. The previous power density was $5\text{ mW}/\text{cm}^2$ and produced an efficiency of approximately 14%. The lens allowed the power density to be increased to $100\text{ mW}/\text{cm}^2$ and the measured output at 0.53μ was 0.6 watts with mode-locking and 0.3 watts without mode locking. Therefore, after increasing the power density by a factor of 20 the efficiency remained constant at approximately 14% indicating a saturated condition. The crystal surface



was very lightly damaged after approximately 60,000 pulses at a power density of 100 mW/cm^2 (not including the mode-locking pulse amplitude enhancement).

4.1.3 SHG with Cesium Dideuterium Arsenate

A one cm cube of CD*A was inserted into the oven in place of the lithium niobate and brought up to phase-match temperature slowly (since another crystal had fractured due to cooling too rapidly in another test). At full power input and at 100 pps the average output power at 0.53μ was 0.7 watts mode-locked and 0.35 watts unmode locked. The power density was the same as with lithium niobate at 100 Mw/cm^2 . During the next series of tests the power density was slowly increased to 200 MW/cm^2 at which point the average output power at 0.53μ had increased to 1.8 watts mode locked and 0.6 watts unmode-locked showing the highest efficiency yet obtained, 25% of the polarized output. The repetition rate was slowly increased from 100 pps to 200 pps producing an average output of 2.8 watts at 0.53μ . During subsequent tests the repetition rate was increased further to 800 pps at which point the average output at 5300 \AA was a stable 6 watts. By allowing the temperature to drift through the phase-match temperature an output of 7.2 watts was observed at 800 pps. The difference (see Fig. 4-8) between the efficiency observed at 100 pps (25%) and 800 pps (12%) can be attributed entirely to the temperature difference across the beam within the CD*A crystal caused by the absorption at 1.06 microns (See Paragraph 5-2). Only a very slight temperature "hang-up" or thermal runaway was observed at or around the phase-match temperature in CD*A indicating far less two photon absorption than in barium sodium niobate or lithium niobate. The table in Fig. 4-9 tabulates the results obtained in all SHG materials tested.

4.1.4 Improved Mode-Locking Enhancement

During the course of the previous tests it was observed that when mode-locking enhancement was employed the primary effect in SHG enhancement was in the center of the beam instead of the complete beam as one would expect. Since the Series 250 mode-locked CW YAG laser output beam diameter is on the order of 1mm and the Q-switched Series 2500 laser utilizes 1/4 inch diameter rods, it is possible that the beam ratio is approximately preserved and that in fact we are only mode locking the very center of the Q-switched

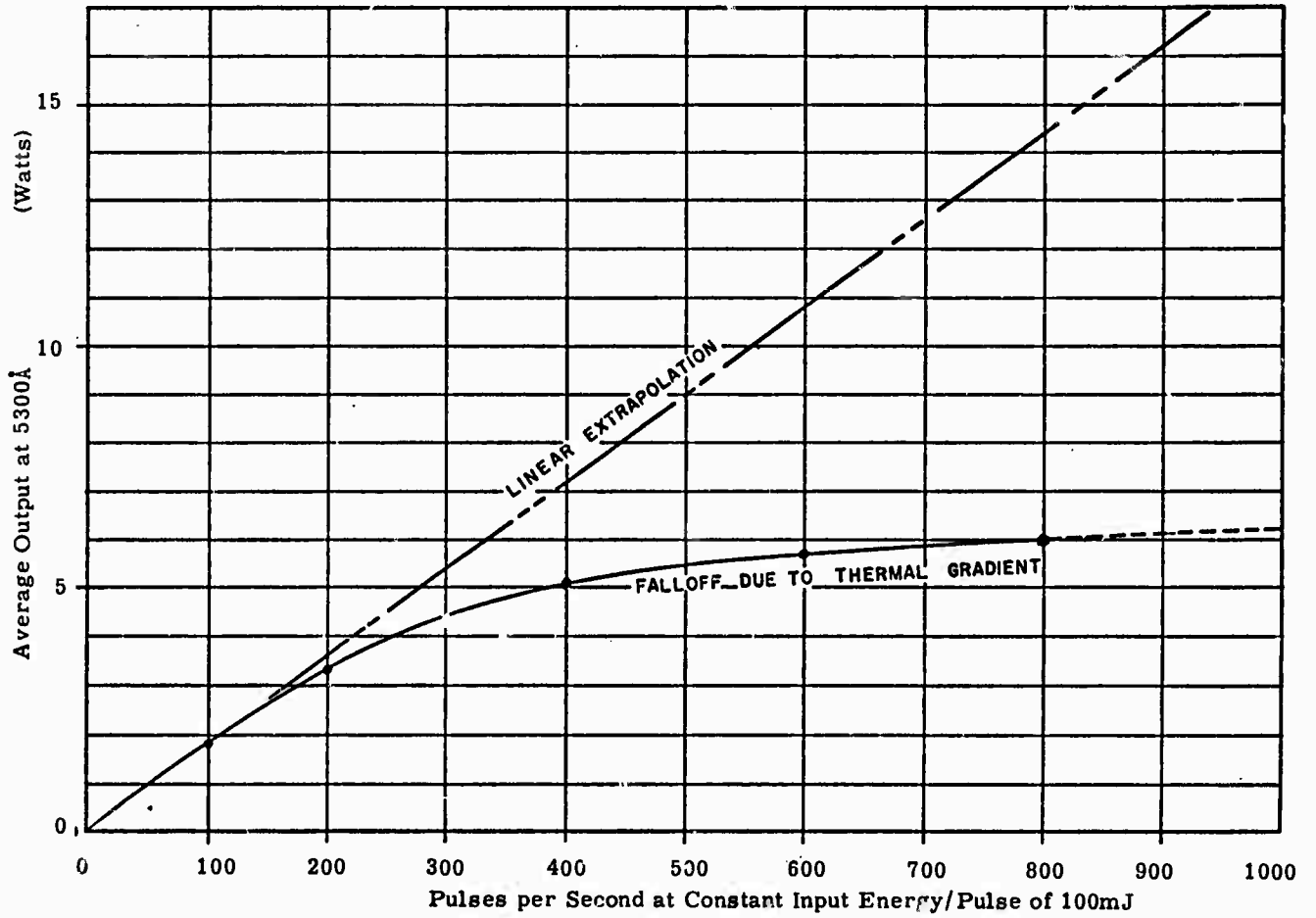


FIGURE 4-8

Average Output versus Pulses per Second

LENGTH	MATERIAL	POWER DENSITY IN MW/cm ²						
		5	M.L. ▲	100	M.L. ▲	200	M.L. ▲	M.L. ▲▲
5 mm	BaNaNb ₅ O ₁₅	12%	6%					
5 mm	LiNbO ₃	7%	14%	7%	12%			
1 cm	CsD ₂ AsO ₄	.1%	1%	4%	12%	10%	25%	40% ▲▲▲
2 cm	KD ₂ PO ₄		.1%			.5%	1.5%	2.5%

- ▲ Low Efficiency Mode Locked
- ▲▲ High Efficiency Mode Locked
- ▲▲▲ Expected Efficiency Based on Results of KD₂PO₄

FIGURE 4-9
Measured Single Pass Efficiency of SHG Materials



output beam. In an effort to determine whether this is occurring a 5:1 up collimator was installed inside the cavity of the CW mode-locked system increasing the injected beam diameter to 5mm. In attempting to evaluate the effect of this larger beam, the CD*A crystal was destroyed, not because of the mode-locking enhancement but because a high rep rate high average power beam was introduced into the crystal too rapidly causing a thermal strain and fracturing the crystal. Since another CD*A crystal was not immediately available, a KD*P crystal (2 cm in length) was installed and the enhancement was checked. Where previously a SHG enhancement ratio of 3 to 1 was typical, the new enhancement ratio is 5 to 1. The KD*P produced an average 0.53μ output of 0.3 watts mode-locked at 100 pps and 0.060 watts non-mode-locked. Increasing the repetition rate to 600 pps produced a linear extrapolation to 1.8 watts average power output at 0.53μ .

- 4.1.5 When it became apparent that the hoped for 2 cm long crystal of CD*A could not be obtained, it was decided to try SHG with two 1 cm crystals in series. Two such crystals were cut from the same boule to insure that their phase-matching temperatures would not differ by more than about one degree centigrade. (The full-width-half-maximum of the temperature tuned phase-matching profile for CD*A was found to be about 5.6°C ; see Section 3.) They were mounted in a cell through which an index matching fluid could be circulated. The fluid itself was heated and temperature controlled to insure a uniform heat zone at the phase-matching temperature. The fluid used was FC-48, a "fluorinert" brand electronic liquid sold by the Chemical Division of the Minnesota Mining and Manufacturing Company.

The best results obtained with the two crystals in series was 0.84 watts at 100 pps; with mode locking this improved slightly to 1.33 watts. Both possible relative orientations of the two crystals were tried. This result was considerably less than expected; a single crystal under similar conditions gave 0.6 and 1.8 watts respectively. Although the poor enhancement with mode locking for the two crystal case might have been due to a degradation of the mode-locked seed pulses, the unmode-locked result showed very little of the increase in conversion efficiency expected from doubling the interaction length.



The most probable reason for this disappointing result was suggested by Fred Quelle. He pointed out that in order for the second crystal to in fact double the effective interaction length, the specific phase relationship between the fundamental and second harmonic fields must be maintained (or incremented by a multiple of 2π) in traversing the fluid between the crystals. Any net phase shift up to $\pm 90^\circ$, would tend to decrease the effectiveness of the second crystal; a larger net phase shift could result in some of the second harmonic power from the first crystal being converted back to the fundamental in the second, i. e., an effective interaction length shorter than that of only one of the crystals.

No refractive index data was available for the particular fluorinert used, FC-48, but an extrapolation of index data for a similar one of the series, FC-75, showed that a phase shift of about 8 radians per mm could be expected between the fundamental and second harmonic due to its dispersion. Since the spacing between the two crystals was about 2mm, this was undoubtedly the reason for the negligible improvement of the second crystal. To make the second one effective, the spacing between the two would have to have been adjustable to an accuracy of about ± 200 microns.

4.1.6 SHG Experiment Conclusions

The data presented in this section clearly indicates that cesium dideuterium arsenate is the only SHG material studied which has any reasonable probability of reaching the basic goals of this development program. At low repetition rates it is reasonable to expect overall efficiencies in excess of 50% by utilizing the 5 to 1 enhancement technique and a 2 cm long crystal at a power density (unmode-locked) of 200 Mw/cm^2 . At high repetition rates the absorption at 1.06 microns will still present a problem in terms of the thermal loading on the crystals and the temperature gradient across the beam.



SECTION V

SOME THEORETICAL CONSIDERATIONS

5.1 Crystal Heating Due to Super Non Linear Effects

Three of the four SHG materials used in the course of these experiments showed unmistakable evidence of some form of absorption process that depended on the presence of the second harmonic field, the one exception being KD_2PO_4 . The evidence was a distinctive crystal heating at the second harmonic phase-matching temperature. Significantly, KD_2PO_4 tunes very slowly with temperature so it is possible that the effect was there but not noticed. In LiNbO_3 and $\text{Ba}_2\text{NaNb}_5\text{O}_{15}$ this heating effect was very severe, and the second harmonic output saturated with increasing fundamental power; in $\text{Ba}_2\text{NaNb}_5\text{O}_{15}$, the second harmonic output actually decreased with an increase in fundamental power, the decrease happening much more quickly than the change in crystal temperature. Since the absorption phenomena which is responsible for this heating in the three crystals may be related, and since it has limited the use of $\text{Ba}_2\text{NaNb}_5\text{O}_{15}$ and LiNbO_3 as high power SHG's, it is of interest to check theoretically for the mechanisms which could be responsible. Attention will be centered on the effect as observed in $\text{Ba}_2\text{NaNb}_5\text{O}_{15}$ since it was most severe in this crystal.

The three main features of the absorption mechanism which have to be contained in a successful theory are.

- 1) The crystal heating and thus the absorption depends on the presence of power in the second harmonic field. This is evidenced by crystal heating only when second harmonic power is being generated in the crystal.
- 2) Relatively large amounts of power are absorbed, approximately 20% of the input power at 6 watts fundamental power input.
- 3) A distinct (by a factor of 2.3) decrease in second harmonic output for an increase in fundamental power. The fundamental power was increased by mode locking the Q-switched laser. Away from the optimum phase-matching temperature, where the second harmonic output was much less, the mode locking enhanced the generated second harmonic power by a factor of three.



Third and Fourth Harmonic Generation

Crystal heating, as characterized by i), has been observed before by others and reported in the literature⁽¹⁾. They attribute it to the generation and subsequent absorption of higher order harmonics of the pumping field. A very important feature of this proposed mechanism is that the power is not absorbed directly, but is first coupled to the higher harmonic fields via the same nonlinearity responsible for the generation of the second harmonic. The implication of this is that any crystal which has a large d coefficient, and thus the potential of being a good second harmonic generator, will also have a severe absorption problem if the next two higher harmonics lie in an absorption band. However, it will be shown below that the power absorbed by the crystal via this mechanism is in fact inversely proportional to the absorption coefficients at the higher harmonic fields. Therefore, it is unlikely that enough power could be absorbed to explain the observed effects. In particular, the best estimates of the amount of power absorbed in $\text{Ba}_2\text{NaNb}_5\text{O}_{15}$ via this mechanism will be shown to be several orders of magnitude too small to account for the observed heating.

To calculate the power absorbed at the higher harmonics, we can use the form of the wave equation used for nonlinear optics as long as the amplitudes of the field vary slowly with respect to their associated k vectors, i. e.,

$$\frac{\partial E_n}{\partial Z} \ll k_n E_n$$

For a lossy region of the spectrum $k \gg \alpha$ where α is the field loss coefficient of the crystal; for visible frequencies, this means $\alpha \ll 10^5 \text{ cm}^{-1}$. Since losses of the order of 10^2 cm^{-1} are very large, this assumption is still good. Therefore, assuming plane waves, the amplitude of the third harmonic field varies as⁽²⁾:



$$\begin{aligned} \frac{1}{2} \left(\frac{\partial E_3}{\partial Z} + \alpha_3 E_3 \right) e^{i(\omega_3 t - k_3 Z)} + \text{C. C.} \\ = - \frac{\mu_0}{i k_3} \frac{\partial^2}{\partial t^2} \left[\frac{d}{2} E_2 E_1 e^{i[(\omega_2 + \omega_1)t - (k_2 + k_1)Z]} + \text{C. C.} \right] \end{aligned} \quad (1)$$

As a worst case limit, we can assume perfect phase matching although we are interested in cases where the fundamental and the second harmonic (and therefore not the third harmonic) are phase matched. This gives,

$$\frac{dE_3}{dZ} + \alpha_3 E_3 = -i \mu_0 \frac{\omega_3^2}{k_3} d E_1 E_2 \quad (2)$$

solving for $|E_3|$ only, and neglecting depletion of E_1 and E_2 ,

$$\frac{dE_3}{2K_3 E_1 E_2 - \alpha_3 E_3} = dZ$$

at $Z = 0$, $E_3 = 0$

$$\therefore E_3 = \frac{2K_3 E_1 E_2}{\alpha_3} (1 - e^{-\alpha_3 Z}) \quad (3)$$

$$\text{where } K_3 = \frac{\mu_0 d \omega_3^2}{2 k_3}$$

Converting to power,

$$P_3 = P_{30} (1 - e^{-\alpha_3 Z})^2 \quad (4)$$



$$\text{where } P_{30} = \frac{A}{2\eta_3} \left(\frac{2K_3 E_1 E_2}{\alpha_3} \right)^2$$

η_3 = crystal impedance at 3rd harmonic

A = cross sectional area of beam

Thus, the power in the third harmonic field grows quadratically with distance at first, but saturates at P_{30} in a distance $Z \approx \frac{1}{\alpha_3}$. In fact,

P_{30} is exactly the amount of power that would be generated in the absence of absorption in a crystal of length = $\frac{1}{\alpha_3}$. After this distance,

there is an equilibrium between the power added by harmonic generation and the power absorbed by the crystal. Since the power absorption at the third harmonic is $2 \alpha_3$, the power absorbed in an incremental distance ΔZ after this saturation regime is reached is given by:

$$P_3 (\text{absorbed in } \Delta Z) = P_{30} (1 - e^{-2 \alpha_3 \Delta Z})$$

$$P_3 (\text{absorbed in full crystal}) = \lim_{\Delta Z \rightarrow 0} \left(P_{30} (1 - e^{-2 \alpha_3 \Delta Z}) \frac{\Delta Z}{\Delta Z} \right)$$

$$P_3 (\text{abs}) = 2P_{30} \alpha_3 \ell \tag{5}$$

where α_3 = field abs. coefficient

ℓ = crystal length. It is assumed that $\ell \gg \frac{1}{2\alpha_3}$.

Substituting for P_{30} and K_3 ,

$$P_3 (\text{abs}) = 4 \omega_3^2 d^2 \eta_1 \eta_2 \eta_3 \frac{P_1 P_2}{A} \frac{\ell}{\alpha_3} \tag{6}$$

Similar results are obtained for the absorbed power due to doubling the second harmonic:

$$P_4 (\text{abs}) = 2 P_{40} \alpha_4 \ell \tag{7}$$

$$= \omega_4^2 d^2 \eta_2^2 \eta_4 \frac{P_2^2}{A} \frac{\ell}{\alpha_4} \tag{8}$$



These results show that the total absorption due to the generation of fields at the higher harmonics is inversely proportional to the absorption coefficient at that frequency.

Unfortunately, these absorbed powers cannot be calculated directly because the values of the electro-optic constant and refractive indices are not known in the absorption region (3).

For absorption due to lattice transitions, it has been shown both experimentally and theoretically by Henry and Garrett⁽³⁾ that both d and α become resonantly large near the resonant frequency in some types of crystals. The transition of interest in $\text{Ba}_2\text{NaNb}_5\text{O}_{15}$ is electronic not vibrational so it is not obvious that it affects d , but it does have a large effect on n . However, an approximate value of these absorbed powers can be obtained from equation (5) and (7) using data from reference (1). Here the authors measured the energy at the third and fourth harmonics that was generated in the last coherence length during phase-matched SHG in $\text{Ba}_2\text{NaNb}_5\text{O}_{15}$. These results are:

$$E_{30}/E_2 = 10^{-6}$$

$$E_{40}/E_2 = 2 \times 10^{-6}$$

Using equations (6) and (8), and the pulse data from this reference, P_{30} and P_{40} can be normalized in terms of P_1 , P_2 , and A .

$$P_{30} = 2 \times 10^{-8} \text{ w/pulse} = 5 \times 10^{-22} \frac{\text{cm}^2}{\text{w}} \times \frac{P_1 P_2}{A}$$

$$P_{40} = 4 \times 10^{-8} \text{ w/pulse} = 2.5 \times 10^{-21} \frac{\text{cm}^2}{\text{w}} \times \frac{P^2}{A}$$

In the same reference, the following approximate values of α_3 and α_4 were obtained.

$$\alpha_3 = 7.5 \text{ cm}^{-1}$$

$$\alpha_4 \gg \alpha_3$$

(9)



From the experimental results obtained here in $\text{Ba}_2\text{NaNb}_5\text{O}_{15}$,

$$P_1 (\text{aver}) = 6 \text{ w @ } 100 \text{ pps.}$$

$$P_2 (\text{aver}) = 0.7 \text{ w @ } 100 \text{ pps.}$$

$$\text{Q-switched pulsewidth} = 30 \text{ ns}$$

$$\text{Mode-locking enhancement} = 3$$

$$\text{Crystal length} = l = 0.5 \text{ cm}$$

This gives

$$P_3 (\text{abs}) \simeq 60 \text{ uw @ } 100 \text{ pps.}$$

$$P_4 (\text{abs}) \simeq 4. \text{ mw @ } 100 \text{ pps.}$$

where we have assumed $\alpha_4 = 10^3 \alpha_3 \simeq 7.5 \times 10^3 \text{ cm}^{-1}$ to comply with equation 9 and give a reasonable upper bound on $P_4 (\text{abs})$. Thus, even for this tremendously large value of α_4 , the powers absorbed via this mechanism of harmonic generation do not come close to the observed 1.1 watts.

Multi-Photon Absorption

Another possible explanation of the observed heating effect is direct multi-photon absorption of fundamental and second harmonic power. This is to be contrasted with the previously discussed absorption. In this case the absorption does not depend on the generation of higher harmonic fields which must be subsequently absorbed, rather the fundamental and second harmonic photons are absorbed directly.

To get an idea of the effect on SHG of this direct multi-photon absorption, it will be introduced phenomenologically into the wave equation via the induced polarizability. The same approximations can be used to simplify the wave equation as are used for analyzing parametric interactions, since the observed effect has approximately the same magnitude. Neglecting linear loss, the steady state wave equation then becomes:



$$ik_n \frac{dE_n}{dZ} e^{i(\omega_n t - k_n Z)} + C. C. = -\mu_0 \frac{\partial^2}{\partial t^2} \left[P_n^{N. L.} (Z_1, t) \right] \quad (10)$$

where the subscript n refers to a particular Fourier component of the electric or polarization field. The term $P_n^{N. L.}$ includes only nonlinear terms in the electric field, the linear term having been included in the L. H. S. The total induced polarizability can be written:

$$P = \chi E + dE^2 + fE^3 + gE^4 + hE^5 + \dots \quad (11)$$

To find which terms are responsible for multi-photon absorption, the term in Poyntings Theorem for the power expended in polarizing the dielectric can be used (4):

$$\text{Power lost} = E \overline{\frac{\partial P}{\partial t}} \quad (12)$$

where the bar indicates a time average over the harmonic frequency. Substituting equation 11 into 12,

$$\text{Power lost} = \sum_n i\omega_n (\chi E^2 + dE^3 + fE^4 + gE^5 + hE^6 + \dots)_n$$

where the subscript n denotes only those terms which vary at the harmonic frequency ω_n . From this it is apparent that the imaginary parts of the coefficients of E^2 , E^4 , and E^6 give rise to one, two, and three photon absorption. Therefore, a polarization and electric field of the following form will be assumed:

$$P^{N. L.} = dE^2 - ifE^3 - ihE^5 \quad (13)$$

$$E(Z_1, t) = \frac{1}{2} \left[E_1(Z) e^{i(\omega_1 t - k_1 Z)} + E_2(Z) e^{i(\omega_2 t - k_2 Z)} + C. C. \right] \quad (14)$$

where the subscripts refer to the first and second harmonics, and the amplitudes can in general be complex. The term for single-photon absorption (linear loss) has been left out because the form of the resulting solution, namely:

$$E_2 = \frac{KE_1^2}{\alpha_2} (1 - e^{-\alpha_2 Z})$$

does not exhibit a saturation with increasing E_1^2 as shown by the experimental result.



To find the driving polarization for the SH field, substitute equation 13 into 14, and assume that only the second harmonic process is phase matched, i. e. ,

$$\omega_2 = 2\omega_1$$

$$k_2 = 2k_1$$

Thus all terms in equation 12 at different frequencies than ω_2 or $2\omega_1$ can be ignored. Substituting the resulting second harmonic polarization into equation 10 gives:

$$\frac{dE_2}{dZ} = -iKE_1^2 - \alpha_1 |E_1|^2 E_2 - \alpha_2 |E_1|^4 E_2 \quad (15)$$

where

$$K = \eta_1 \omega_1 d$$

$$\alpha_1 = 3\eta_1 \omega_1 f$$

$$\alpha_2 = \frac{15}{4} \eta_1 \omega_1 h$$

Note that the second term on the R. H. S. represents two photon absorption, one fundamental and one second harmonic; and the third term represents three photon absorption, two fundamental and one second harmonic. Other absorption terms involving two second harmonic photons have been ignored with respect to these because $(E_1)^2 \approx 10(E_2)^2$.

To simplify the analysis, we will neglect pump depletion; i. e. , assume $E_1 = \text{const}$. This is a good assumption in our case because the observed conversion efficiencies were always less than about 15%.

Note that the field amplitudes are, in general, complex quantities and a solution with a phase variation in Z is conceivable. However, if a solution with no phase variation is possible, it will dominate because the gain mechanism will not be divided to drive both amplitude and phase. Therefore, we will look for a solution with stationary phase. Rewriting E_1 as



$$E_1 = E_{10} e^{i\varphi_1} = \text{Constant}$$

and still allowing $E_2(Z)$ to be complex, eq. (15) becomes

$$\frac{dE_2}{dZ} = KE_{10}^2 e^{i(2\varphi_1 - \pi/2)} - (\alpha_1 E_{10}^2 + \alpha_2 E_{10}^4) E_2 \quad (16)$$

From this it is evident that a stationary phase solution exists of the form:

$$E_2(Z) = E_{20}(Z) e^{i(2\varphi_1 - \pi/2)}$$

where $E_{20}(Z)$ is real. With this addition, the equation becomes:

$$\frac{dE_{20}}{dZ} = KE_{10}^2 - (\alpha_1 E_{10}^2 + \alpha_2 E_{10}^4) E_{20}$$

This can be easily integrated, giving

$$E_{20} = \frac{1}{\alpha_1 E_{10}^2 + \alpha_2 E_{10}^4} \left[KE_{10}^2 - C e^{-(\alpha_1 E_{10}^2 + \alpha_2 E_{10}^4) Z} \right]$$

The boundary condition is that @ $Z = 0$, $E_2 = 0$. Thus,

$$C = KE_{10}^2$$

Using (17) to write the total solution,

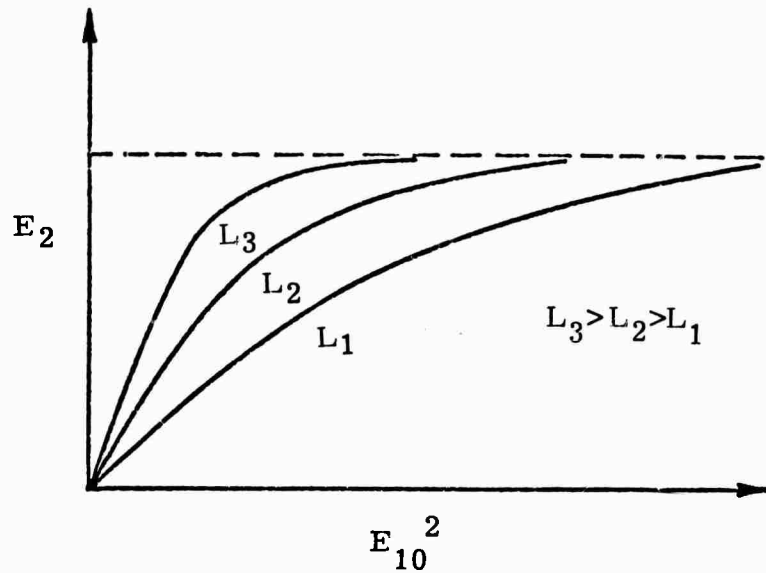
$$E_2(Z) = \frac{K}{\alpha_1 + \alpha_2 E_{10}^2} \left[1 - e^{-(\alpha_1 E_{10}^2 + \alpha_2 E_{10}^4) Z} \right] e^{i(2\varphi_1 - \pi/2)} \quad (17)$$

To understand this solution, assume first that $\alpha_2 E_{10}^2$ is negligible with respect to α_1 . Then the solution reduce to:

$$E_2 = \frac{K}{\alpha_1} \left[1 - e^{-\alpha_1 E_{10}^2 Z} \right] e^{i(2\varphi_1 - \pi/2)} \quad (18)$$



The magnitude of E_2 for this case is plotted below versus E_{10}^2 for three different crystal lengths $Z = L$.



Note that this result implies a saturation of the generated second harmonic field at a value of $E_2 = \frac{K}{\alpha_1}$ which is determined solely by the crystal parameters.

For the general case, equation 17 can be normalized as follows:

$$y = \frac{1}{1 + \chi} \quad 1 - e^{-\chi(\chi + 1)L}$$

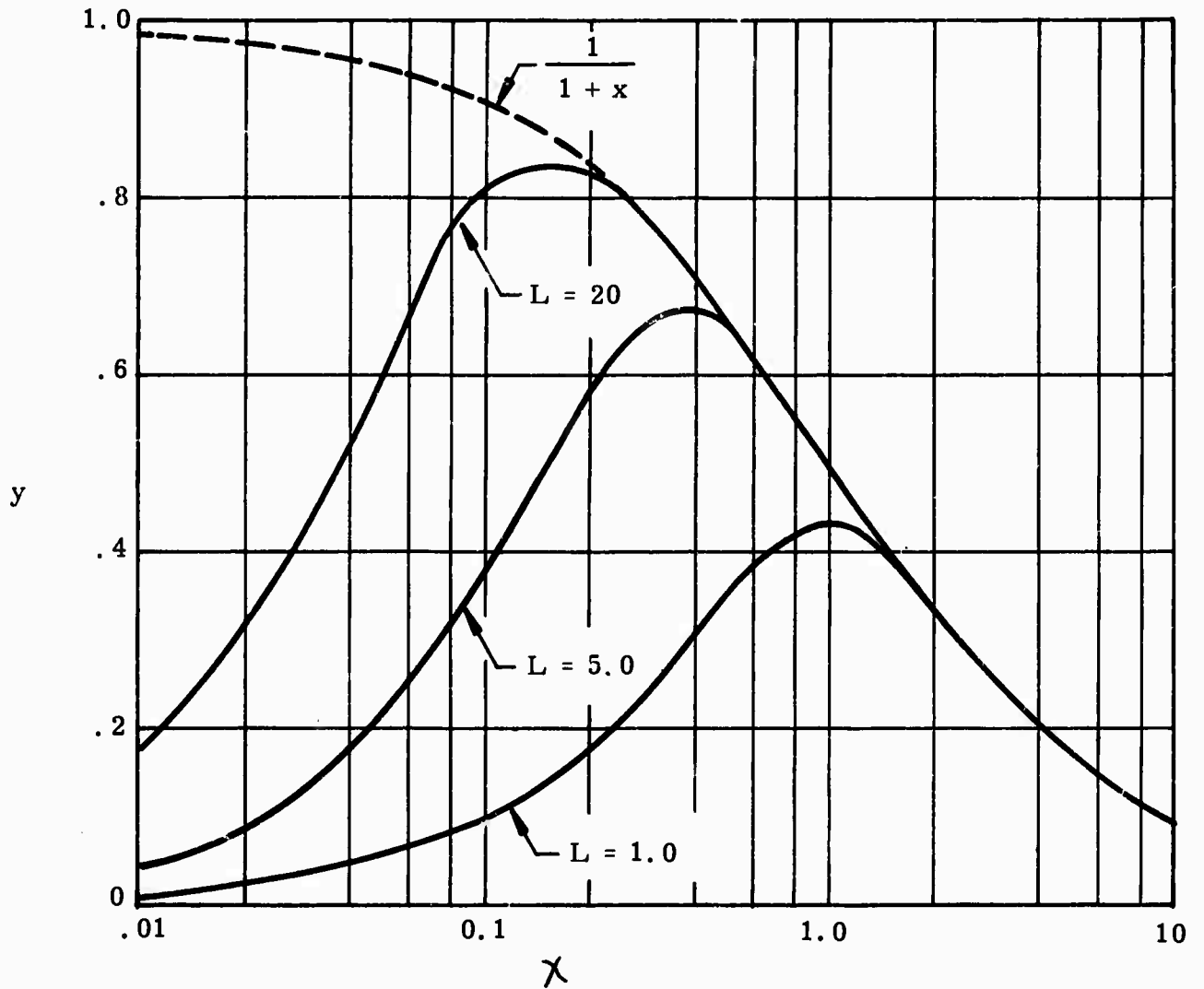
where

$$y = \frac{\alpha_1}{K_1} E_{20}$$

$$\chi = \frac{\alpha_2}{\alpha_1} E_{10}^2$$

$$L = \frac{\alpha_1^2}{\alpha_2} Z$$

This is graphed below.



In this plot the maximum value for E_2 is again $E_2 = \frac{K}{\alpha_1}$ but it occurs only for large values of the length parameter L and at a specific E_{10}^2 . Also, this solution shows a decrease in E_2 with increasing E_{10}^2 which was not true for the case of $\alpha_2 = 0$.



Discussion of Theoretical Results

Any loss mechanism which results in the second harmonic output saturating at less than 100% conversion can exhibit a decrease in second harmonic output due to mode locking. If the un-mode locked fundamental is enough to reach the second harmonic saturation level, the increased peak power due to mode locking will not produce more peak second harmonic power; averaging over the mode-locking period will then give an output less than the saturated second harmonic level.

If we assume that two photon absorption is responsible for the observed saturation effects, i. e., equation 18, we can calculate the expected decrease in average second harmonic power due to the introduction of mode locking.

Assume the mode-locked fundamental has the following time waveform

$$P_1(t) = P_1 e^{-a^2 t^2} \tag{19}$$

where P_1 is the peak power of the mode-locked pulse, and a is related to the second harmonic enhancement, R , due to mode locking (away from saturation) by:

$$a = 2\sqrt{2} R \Delta f_{ax} \tag{20}$$

from equation 19,

$$P_2(t) = P_2(\text{sat}) \left[1 - e^{-\alpha_1 E_{10}^2(t) Z} \right]^2$$

where

$$P_2(\text{sat}) = 2\eta A \left(\frac{K}{\alpha_1} \right)^2$$

Taking the average over time,

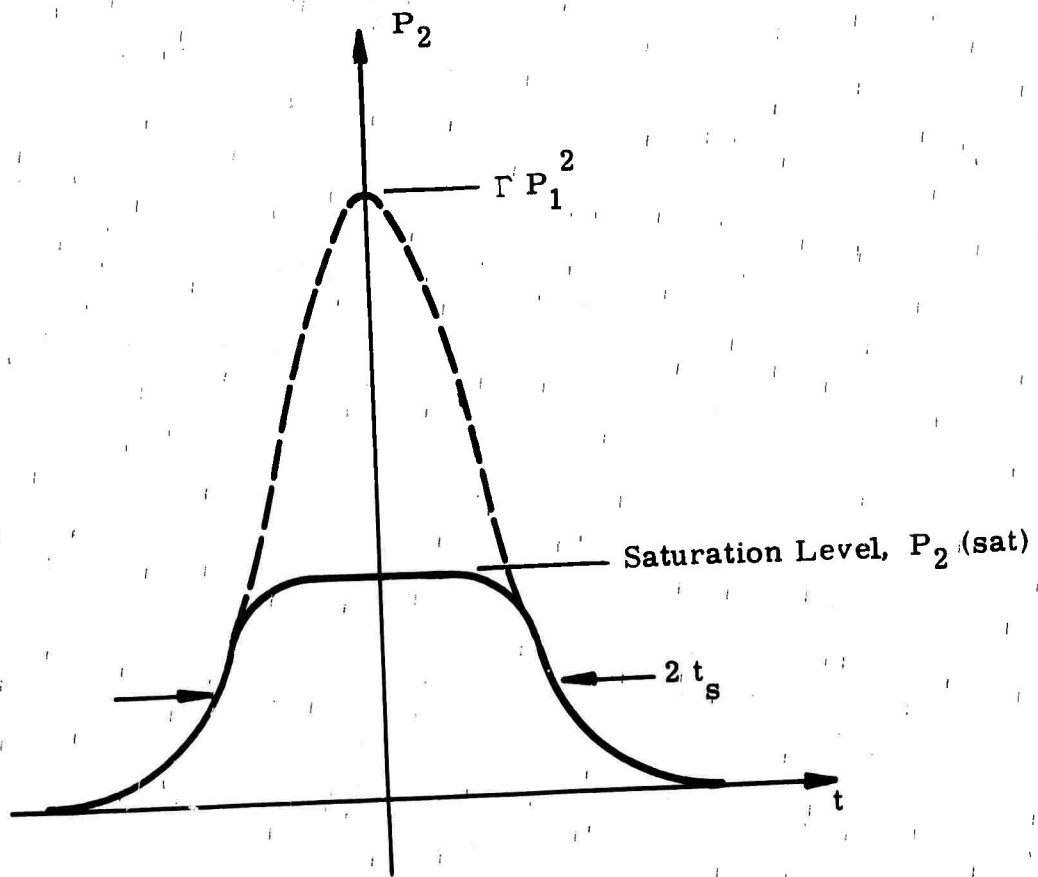
$$P_2(\text{aver, mode-locked}) = P_2(\text{sat}) \Delta f_{ax} \int_{-\infty}^{\infty} \left[1 - e^{-\alpha_1 E_{10}^2(t) Z} \right]^2 dt \tag{21}$$

where E_{10}^2 is given by equation 19. Rather than trying to perform this integration analytically, it will be approximated as follows.

Away from saturation, the fundamental and second harmonic are related by:

$$P_2(t) = \Gamma P_1^2(t) = \Gamma P_1 e^{-2a^2 t^2} \tag{22}$$

This Gaussian waveform is shown by the dashed curve in the plot on the next page.



Referring to this plot it can be seen that t_s can be related to $P_2(\text{sat})$ as follows: /



For a saturation level less than ΓP_1^2 , the resulting waveform will be more like that indicated in the figure by the solid line. Therefore, equation 21 reduces to

$$P_2 \text{ (average, mode-locked)} = 2t_s P_2(\text{sat}) \Delta f_{ax} \quad (23)$$

where

$P_2(\text{sat})$ = maximum SH power level as a result of 2-photon absorption.

$2 t_s$ = FWHM of saturated, mode-locked SH pulse.

Δf_{ax} = mode-locking frequency.

$$\frac{P_2(\text{sat})}{2} = \Gamma P_1^2 e^{-2a^2 t_s^2}$$

$$t_s = \left[-\frac{1}{2} \ln \frac{P_2(\text{sat})}{2\Gamma P_1^2} \right]^{\frac{1}{2}} \quad (24)$$

Combining equations 23, 24 and 20,

$$P_2 \text{ (ave, m.l.)} = \frac{P_2(\text{sat})|_{\text{average}}}{\sqrt{2} R} \left[-\frac{1}{2} \ln \frac{P_2(\text{sat})}{2\Gamma P_1^2} \right]^{\frac{1}{2}} \quad (25)$$

where this is now averaged over both mode locking and Q-switching.

For a $Ba_2NaNb_5O_{15}$ crystal of length 0.5 cm and for a beam diameter of 3/16", the Γ of equation 22 is:

$$\Gamma = 1.3 \times 10^{-6} \text{ watt}^{-1}$$

From the experimental data,

$$P_2(\text{sat})|_{\text{average}} @100\text{pps} = 0.7 \text{ watts}$$

$$\text{SH pulse width} = \text{fundamental Q-switched width} = 30 \text{ ns.}$$

$$P_1 \text{ average} @100\text{pps} = 6.0 \text{ watts}$$

$$R = \text{Mode-locking enhancement} = 3$$



Therefore,

$$P_2(\text{sat}) = 0.22 \text{ Mw}$$

$$P_1(\text{peak}) = 17 \text{ Mw}$$

Substituting these values into equation 25 gives:

$$P_2(\text{av, m.l.}) = 0.335 \text{ watts.}$$

This is in good agreement with the experimentally obtained result, 0.30 watts.

The good agreement obtained above indicates that the observed saturation phenomena is well accounted for by a direct 2-photon absorption process, one fundamental and one second harmonic, which gives a second harmonic field of the form shown in eq. (18) and the plot on page 59. If the three-photon process were significant, a smaller value of $P_2(\text{av, m.l.})$ would be predicted because of the decrease in E_2 for larger value of E_{10}^2 .

A theoretical estimate of the power absorbed by the two photon process is also possible. To perform the calculation the wave equation for the fundamental electric field is needed as well as that for the second harmonic field. It can be derived in a manner similar to that of equation 15; the result is:

$$\frac{dE_1}{dZ} = -iKE_2E_1^* - \frac{\alpha_1}{2} |E_2|^2 E_1 \quad (26)$$

where α_1 , and K are as previously defined.

From this and equation 15,

$$E_1 \frac{dE_1^*}{dZ} = \frac{1}{2} \frac{d|E_1|^2}{dZ} = iKE_2^*E_1^2 - \frac{\alpha_1}{2} |E_2|^2 |E_1|^2$$

$$E_2^* \frac{dE_2}{dZ} = \frac{1}{2} \frac{d|E_2|^2}{dZ} = iKE_1^2E_2^* - \alpha_1 |E_1|^2 |E_2|^2$$

Adding these two and rewriting in terms of power,

$$\frac{d}{dZ} (P_1 + P_2) = -3\alpha_1 |E_2|^2 P_1 \quad (27)$$



Thus, the R. H. S. gives the rate at which power is being taken from the first and second harmonic fields with distance. Integrating over Z gives the total power absorbed by the crystal per pulse. Since P_1 was assumed constant with distance to derive $E_2(Z)$, the same assumption will be used here. Substituting equation 26 into 27 and integrating,

$$\begin{aligned}
 P(\text{abs}) &= 3 \frac{K^2}{\alpha_1} P_1 \int_0^l dZ \left[1 - e^{-\alpha_1 E_{10}^2(t) Z} \right]^2 \\
 &= 3 \frac{K^2}{\alpha_1} l P_1 - 6 P_2(\text{sat}) \left[1 - e^{-\alpha_1 E_{10}^2(t) l} \right] \\
 &\quad + \frac{3}{2} P_2(\text{sat}) \left[1 - e^{-2\alpha_1 E_{10}^2(t) l} \right] \tag{28}
 \end{aligned}$$

To relate this to the experimental results, it must be averaged over both the mode locking and the Q-switching periods. Averaging the second and third terms over the mode-locking period results in integrals very similar to that of equation 29. Estimating their value from that result, equation 28 becomes:

$$P(\text{abs}) \simeq 3 \frac{K^2}{\alpha_1} l (P_1)_{\text{average}} - 3 (P_2(\text{sat}))_{\text{average}}$$

From the experimental results,

$$(P_2(\text{sat}))_{\text{average}} = 0.7 \text{ watts}$$

$$(P_1)_{\text{average}} = 6.0 \text{ watts}$$

$$\frac{K}{\alpha_1} = E_2(\text{sat}) = 2 \times 10^6 \text{ V/m}$$

$$l = 0.5 \times 10^{-2} \text{ m}$$

For $\text{Ba}_2\text{NaNb}_5\text{O}_{15}$

$$K = \eta_1 \omega_1 d = 4 \times 10^{-5} / \text{volt}. \tag{29}$$

Substituting those values gives

$$P(\text{abs}) = 7.2 - 2.1 = 5.1 \text{ watts} \tag{30}$$



This is about five times greater than the observed power absorption. Note, however, that any flaws in the $Ba_2NaNb_5O_{15}$ crystal, temperature gradients in the crystal due to this absorption or non-uniformities in the oven, or non-uniformities in the pumping field from higher order transverse modes will decrease the effective value of the d coefficient in equation (29). All other parameters used to obtain (30) were directly measured and therefore already reflect the effective rather than the highest possible value for d .

The significant thing that this calculation shows is that the suggested mechanism for absorption is of the correct order of magnitude to account for the observed absorption.

Conclusions

The most important conclusions of this two-photon absorption theory are that the second harmonic electric field saturates below 100% conversion, and that the maximum value for this saturation level is inherent to the crystal and represents a fundamental limitation to power density conversion efficiency. The value obtained for the $Ba_2NaNb_5O_{15}$ crystal used here is $E_2(\text{sat}) = 2 \times 10^6 \text{V/m}$. This converts to the following power density:

$$\frac{P_2}{A} (\text{sat}) = 1.2 \frac{\text{Mw}}{\text{cm}^2}$$

Therefore:

- i) To obtain high power conversion efficiencies and more total second harmonic, relatively long crystals and lower power density beams are required.
- ii) To avoid heating and possible damage, the fundamental power density should be kept below that required to reach saturation, since power density above this level yields no more second harmonic power and leads to excessive absorption.



5.2 Phase-Match Degradation Due to Absorption

Absorption of laser radiation in the SHG crystal creates a temperature profile across the beam region, making it impossible to maintain perfect 90° phase-matching over the entire beam cross section. We have seen this effect clearly both in low power CW SHG with Ba₂NaNb₅O₁₅ and high power SHG with CsD₂AsO₄. A calculation of the expected degradation in second harmonic conversion efficiency as the laser average power is increased is presented here.

Our experiments were conducted with a square crystal with a heat sink on only one side. We simplify this geometry for computation purposes to be an infinite cylindrical crystal with a heat sink on the entire surface, with the beam centered on the cylinder axis. We also assume constant power density in the beam. In this case we have a temperature profile over the beam.

$$T(r) = T_0 + \underbrace{\frac{\Delta T_c}{4\pi k} \left[1 + 2\mu n \frac{R}{\omega_0} - \frac{r^2}{\omega_0^2} \right]}_{T_A}$$

$$= T_A - \Delta T_c \frac{r^2}{\omega_0^2}$$

- where
- r = distance from crystal-beam center
 - ΔT_c = temperature differential across beam
 - P = Laser power (watts)
 - β = absorption coefficient (cm⁻¹)
 - k = thermal conductivity (watts °C⁻¹ cm⁻¹)
 - R = crystal radius
 - ω_0 = beam radius



The relative SHG conversion efficiency as a function of temperature is $G(T)$, nominally a $\sin^2 x/x^2$ form.

$$P(2\omega) = a \int_0^{\omega_0} 2\pi r G[T(r)] dr$$

For arithmetic ease we assume that

$$G(T) = e^{-\sigma^2 (T-T_M)^2}$$

where T_M = phase-match temperature

$$P(2\omega) = a \int_0^{\omega_0} r e^{-\sigma^2 \left(T_A - T_M - \Delta T_c \frac{r^2}{\omega_0^2} \right)^2} dr$$

Assume $T_A = T_M$, implying exact phase-match at the crystal center.

yielding

$$\frac{P(2\omega)}{P_0(2\omega)} = \left(\frac{\pi}{8 \ln 2} \right)^{\frac{1}{2}} \left(\frac{\Delta T_M}{\Delta T_c} \right) \operatorname{erf} \left(2 \ln^{\frac{1}{2}} 2 \frac{\Delta T_c}{\Delta T_M} \right)$$

where $\Delta T_M = \frac{2 \ln^{\frac{1}{2}} 2}{\sigma}$ = full width at $\frac{1}{2}$ maximum

$P_0(2\omega)$ = low rep rate (no thermal effect) green power

since $\Delta T_c = \frac{P(\omega) \beta}{2\pi k}$

if we define η as the low rep rate efficiency

$$P(2\omega) = \eta \left(\frac{\pi^3}{2 \ln 2} \right)^{\frac{1}{2}} \frac{\Delta T_M k}{\beta} \operatorname{erf} \left(\frac{\ln^{\frac{1}{2}} 2}{\pi k} \frac{P(\omega) \beta}{\Delta T_M} \right)$$

Since $\operatorname{erf}(x) \rightarrow 1$, the average second harmonic power saturates at a
 $x \rightarrow a$



level

$$P_{\max}(2\omega) = \eta \left(\frac{\pi^3}{2 \ln 2} \right) \frac{\Delta T_M k}{\beta}$$

e.g.

$$\eta = 0.25$$

$$\Delta T_M = 5.6^\circ\text{C}$$

$$k = 0.018 \text{ (estimated for CD*A) watts } ^\circ\text{C}^{-1} \text{ cm}^{-1}$$

$$\beta = 0.009 \text{ cm}^{-1}$$

$$P_{\max}(2\omega) = 0.25 (4.7) (5.6) \frac{(1.8) \times 10^{-2}}{0.9 \times 10^{-2}}$$

$$P_{\max}(2\omega) = 13.2 \text{ watts}$$

The observed saturation level was approximately 8 watts. The 30% disagreement can be explained qualitatively by the fact that the crystal had a heat sink on only one side, causing a larger normal gradient. Further, the exact mathematical form of the phase-match curve should be used in the calculations. The results would also be modified if we took into account saturation in the conversion process.

We conclude from this brief exercise that theoretically we can expect to observe a saturation in the average second harmonic power, the saturation level depending linearly on the phase-match temperature half width and the thermal conductivity and inversely on the absorption coefficient. Our experimental results confirm the calculations, at least approximately, and give support to our understanding of the limitations on harmonic conversion efficiency at high average powers.

5.3 Pulse Width Degradation

A short pulse transmitted through an amplifier with finite bandwidth will suffer an increase in pulse-width. In order to determine the limitations of the mode-locked pulse injection technique we will calculate the theoretical pulse broadening which occurs in the four-five transits through the high gain CW regenerative amplifier.



A Gaussian pulse is assumed, having an amplitude

$$f_1 = \exp [-\alpha t^2]$$

propagated through an amplifier medium with complex gain

$$G(\omega) = \exp \left\{ g_0 \left[1 - jT_2 (\omega - \omega_0) - T_2^2 (\omega - \omega_0)^2 \right] \right\}$$

yielding a new pulse, obtained by Fourier transformation

$$f_2 = \int G(\omega) g(\omega) e^{j\omega t} d\omega$$

where

$$\begin{aligned} g(\omega) &= \frac{1}{2\pi} \int \exp [-\alpha t^2 + j(\omega_0 - \omega)t] dt \\ &= \frac{1}{2\pi} \frac{1}{\alpha} \exp \left[-\frac{(\omega - \omega_0)^2}{4\alpha} \right] \end{aligned}$$

yielding

$$f_2 = \frac{e^{g_0} e^{j\omega_0 t}}{(1 + 4\alpha g_0 T_2^2)^{\frac{1}{2}}} \exp \left[\frac{-\alpha (t - g_0 T_2)^2}{1 + 4\alpha g_0 T_2^2} \right]$$

Ignoring the phase term, we see that the new pulse has a modified Gaussian shape parameter

$$\alpha + \Delta\alpha = \frac{\alpha}{1 + 4\alpha g_0 T_2^2}$$

Since $\frac{2^{\frac{1}{2}}}{\pi} \frac{1}{T_2} = \Delta f_{at}$ = atomic line width

and $\tau_{\frac{1}{2}} = 2^{\frac{1}{2}} \ln 2 \alpha^{-\frac{1}{2}}$ = pulse-width

$$\frac{\Delta\tau_{\frac{1}{2}}}{\tau_{\frac{1}{2}}} = \frac{2 \ln^2 2}{\pi^2} \frac{g_0}{(\Delta f_{at} \cdot \tau_{\frac{1}{2}})^2}$$



For one pass of a 0.2 nanosecond pulse through the amplifier (round trip).

$$\begin{aligned}g_o &= 6 \\ \Delta f_{at} &= 1.6 \times 10^{11} \text{ Hz} \\ \tau_{\frac{1}{2}} &= 2 \times 10^{-10} \\ \frac{\Delta \tau_{\frac{1}{2}}}{\tau_{\frac{1}{2}}} &= 0.00058\end{aligned}$$

In 5 transits the maximum fractional increase in pulse-width is

$$\left(\frac{\Delta \tau_{\frac{1}{2}}}{\tau_{\frac{1}{2}}} \right)_5 = 0.003$$

The effect would be larger for shorter pulses, but we do not anticipate achieving a pulse width shorter than about 0.12 nanoseconds in the long 77MHz cavity. Therefore pulse broadening due to the amplifier bandpass can be neglected.



SECTION VI

CONCLUSIONS

From the results of the program we can conclude:

1. Mode-locked pulse injection combined with Q-switching in a CW high power Nd:YAG laser can be made to function reproducibly, creating substantial increases in laser peak power, which in turn yields a substantial enhancement in second harmonic conversion efficiency.
2. We have demonstrated that by using cesium dideuterium arsenate we can obtain harmonic conversion efficiencies of 25% to 40% with a multitransverse mode laser through the use of 90° phase matching.
3. We have demonstrated a saturation in second harmonic average power resulting from a temperature gradient across the beam due to 1.06 μ absorption.
4. We have discovered what is apparently a fundamental limitation in the use of barium sodium niobate and lithium niobate in the form of a severe thermal heating at conversion efficiencies exceeding a few percent. Evidence points to two photon absorption as the source of this heating.
5. We have produced 7.2 watts at 0.53 microns, approximately a factor of two less than we would have achieved were it not for the thermal gradient effects in the cesium dideuterium arsenate crystal. We have obtained this at a laser pulse repetition frequency of 800 pps, approximately a factor of five slower than the rate at which the laser can be expected to operate with only a slight degradation in pulse peak power.
6. The cesium dideuterium arsenate crystals have been able to withstand the peak powers required to yield high conversion efficiencies of greater than 50%.



The general conclusion that we have reached is that in order to produce average powers at 0.53 microns of greater than 20 watts it will be necessary to take steps to alleviate the thermal limitations of the harmonic generating crystals. This can be accomplished through an improvement in the materials themselves and the use of mechanical techniques which either distribute the thermal loading over a larger crystal volume or improve markedly the rate of heat removal. A discussion of these techniques will be presented in the final report.

It should be possible to obtain an improvement in second harmonic power by approximately a factor of 2.5 by improving the mode-locked pulse injection technique and the polarization characteristics of the laser.

The axial gradient technique which has been applied principally to Nd:Glass and more recently to Nd:YAG lasers attempts to reduce the effect of the thermal input by slicing the active material into many discs, each of which is substantially thinner than the diameter of the area over which the heat is introduced. A coolant, either high velocity gas or a liquid, is passed between the surfaces of the discs, thus producing a temperature gradient which is principally axial rather than radial in direction and is substantially reduced in magnitude. In theory this technique could be applied to the second harmonic generating crystal but there are some trying engineering problems to solve, perhaps even more difficult than those in the axial gradient laser. The temperature control of the crystal is quite critical and therefore a high velocity fluid would be most appropriate. However, due to the dispersion in the fluid, as pointed out in Section II, the phase shift between the fundamental and second harmonic will result in a reduced conversion efficiency unless the distance between the discs is quite small, complicating the problems of high velocity coolant flow. The fluid of course also has to be able to withstand the high peak powers at both the fundamental and second harmonic, must not be aqueous, must have a boiling point above that of the phase-match temperature and must be transparent to the fundamental and second harmonic. The use of a high velocity gas flow would circumvent many of these problems but would add the complications that temperature control is much more difficult and anti-reflection coating or Brewster angle cutting of the crystal discs would be required in order to reduce surface losses since index matching would not be possible. The discs would probably all have to be fabricated from the same boule unless control of



the growth process can be improved to the point where all of the samples have the same phase-matched temperature to well within the half width. Otherwise, the elements would have to be carefully selected from a quantity of boules.

The thermal input to the SHG crystal can conceptually be greatly reduced by using a large crystal volume and rapidly displacing the beam through this volume by mechanical means. As an example, we could build a revolver-like assembly with twenty CD*A "bullets" each embedded in a common heat sink and each selected to have an identical phase-match temperature. Using a prism-mirror arrangement the 1.06 micron beam would pass through each of these crystals in turn, synchronized with the Q-switch repetition frequency of the laser. Again we have the problems of complexity and cost but the probability of producing a functional system seems to be greater with this technique than for the axial gradient method. The theoretical saturation power output for a 20 element system would be greater than 250 watts at 0.53 microns.

Further improvements in the overall efficiency of the laser-SHG system could be obtained by improving the mode-locked pulse injection process through the use of superior electronic techniques and by producing a 100% polarized output beam rather than the partially polarized output now available. The latter can be accomplished through the use of an improved polarizer. Further improvements in the mode-locked pulse injection could be obtained by combining Q-switching and mode locking in the injection oscillator, substantially increasing the energy of the injected pulse, thus guaranteeing saturation of the main regenerative amplifier with negligible contribution from the natural fluorescence.

The theoretical analysis conducted as part of this program has shown reasonable agreement between the experimental evidence and the proposition that direct two photon absorption is responsible for the nonlinear heating effects in the SHG crystals.

The most general conclusion that can be reached is that average powers of at least two hundred watts at 0.53 microns can ultimately be obtained through a combination of the techniques that were studied during this program with improved means for utilizing the SHG crystals and some modifications of the laser source.



SECTION VII

SUGGESTIONS FOR CsD_2AsO_4 CRYSTAL IMPROVEMENT

The single item which would benefit the goals of this program most but was beyond its scope would be a reduction in the absorption coefficient of CD^*A at 1.06 microns by an order of magnitude.

A comparison of the optical transmission curves for deuterated CsD_2AsO_4 and KD_2PO_4 . Figure 3-4 shows a substantially reduced cutoff for CsD_2AsO_4 at both the ultraviolet and infrared ends of the visible spectrum. The fact that ultraviolet transmission for a 1.0 centimeter length of CsD_2AsO_4 is reduced to 50% at 0.24 microns may be an inherent feature of the arsenates versus the phosphates. However, the pronounced dip near 0.35 microns may be due to impurity contamination. At the infrared end greater than twice the absorption at 1.50 microns in CsD_2AsO_4 versus KD_2PO_4 suggest that hydrogen contamination may be present; i. e., the CsD_2AsO_4 sample measured was not as fully deuterated as the KD_2PO_4 sample measured. In fact, it is quite probable that neither sample was fully deuterated. Careful control of the growth parameters for both the tetragonal phosphates and arsenates is therefore imperative if repeatable results are to be ensured.

Since CsD_2AsO_4 has been demonstrated to be a highly important material for 90 degree phase-matched optical frequency doubling of 1.065 micron laser output, it is essential that everything possible be done to improve its optical properties. Dominating these properties presently is the absorption at both 1.054 and 0.533 microns, which must be reduced beyond the current state-of-the-art. Also there are indications that sum-frequency generation may also pose an ultimate thermal limitation upon the material. Since this sum frequency corresponds to a wavelength of 0.355 microns, at the dip in the transmission curve referred to above, it is important to know whether indeed contamination due to growth additives or other chemical impurity is responsible.

A review of several factors influencing CsD_2AsO_4 single crystal growth is presented below. The ultimate aim of a program to improve CsD_2AsO_4 from the standpoint of its optical properties would be to refine each of the growth parameters to a logical and scientifically understood set of operating conditions, thereby removing many of the uncertainties which have kept crystal growing in the realm of a mysterious art.



First, the elimination of all chemical impurities from the starting materials is of utmost importance. Since CsD_2AsO_4 is grown from an acid solution prepared from an admixture of CsAsO_3 in DAsO_3 , there are very few initial ingredients to be checked for purity. Careful control of the cesium salts should be possible by ordinary chemical preparation techniques. Deuterated arsenic acid, derived from the reaction:

$\text{As}_2\text{O}_5 + \text{D}_2\text{O} \longrightarrow 2 (\text{DAsO}_3)$ should be prepared in a dry Argon atmosphere to avoid any possibility of water vapor infiltration. The D_2O itself should be obtainable to better than 99.7% purity from certified government sources.

Second, the growth rate and starting temperature must be judiciously chosen to coincide with the degree of supersaturation both initially and at the end of the growth run. Problems due to tapering of the crystal boules and the inability to sustain a uniform growth rate will adversely affect the optical quality of the finished crystals. Although some experimenters have attempted to introduce trace impurities in order to counter such adverse effects, it is felt that a wiser choice would be to add nothing additional to the growth solution. Rather, a careful search should be made for a temperature regime over which a run could be successfully made without requiring additives. The growth rate achievable under the conditions established above will be determined primarily by the starting temperature and pH factor under optimum supersaturation conditions. Hopefully it will be fast enough to attain an economic yield within three to four months time. Faster growth rates should be avoided since optical homogeneity will suffer if the growing speed is excessive.

Third, thermal gradients and uneven stirring should be avoided since striae and optical index gradations will result. Furthermore, the rotational speed of the crystals, if they are grown in a modified Holden apparatus, should not exceed that required to produce uniform growth along the principal Z-axis direction. While some agitation is necessary, excess or uneven turbulence should be avoided. The physical placement of the growth chamber should be in a room, preferable in a sub-basement location, which will be subject to as little vibration and temperature fluctuation as possible. Adequate insulation and remote electronic temperature control would appear preferable.



Fourth, consideration should be given to the "seed" material which is in the form of carefully prepared 0-degree Z-axis platelets. It is imperative that all residual material be carefully removed from the seed faces to guarantee uniform "capping-over" as the growth is started. Great care must be given to the rate of insertion and temperature of the seeds as they are being lowered into the growing nutrient bath.

Lastly, thorough attention to detail, both in preparation of the nutrient solution and initiation of a growth run will require great patience on the part of the crystal grower. The remainder of the run, lasting for several months, must be fully automated and should include the use of reliable methods of temperature control and an emergency power source to avoid loss of the runs in the event of a local power failure.



REFERENCES

1. W.K. Ng, & E.J. Woodbury, *Ab. Phys., Lett.* 18, 12, 550, (6/15/71).
2. A. Yariv, Quantum Electronics, Wiley & Sons, Inc., N. Y., 1967, pp. 348-350.
3. C.H. Henry & C.G. B. Garrett, *Physical Review* 171, 3, 1058, (68).
4. A. Yariv, Quantum Electronics, Wiley & Sons, Inc. N.Y., 1967, pp. 97.